Calhoun
Institutional Archive of the Naval Postgraduate School

Calhoun: The NPS Institutional Archive

DSpace Repository

Theses and Dissertations | 1. Thesis and Dissertation Collection, all items

1969-12

Design and performance of a twenty-corner-cluster reflector.

Katris, Prokopios

Monterey, California. U.S. Naval Postgraduate School

http://hdl.handle.net/10945/11963

Copyright is reserved by the copyright owner

Downloaded from NPS Archive: Calhoun

DUDLEY KNOX LIBRARY

http://www.nps.edu/library

Calhoun is the Naval Postgraduate School's public access digital repository for research materials and institutional publications created by the NPS community. Calhoun is named for Professor of Mathematics Guy K. Calhoun, NPS's first appointed -- and published -- scholarly author.

Dudley Knox Library / Naval Postgraduate School
411 Dyer Road / 1 University Circle
Monterey, California USA 93943

NPS ARCHIVE
1969
KATRIS, P.

DESIGN AND PERFORMANCE OF A TWENTY-CORNER-CLUSTER REFLECTOR

Prokopios Katris

DUDLEY KNOX LIBRARY
NAVAL POSTGRADUATE SCHOOL
MONTEREY, CA 93943-5101

United States
Naval Postgraduate School

THESIS

DESIGN AND PERFORMANCE OF A
TWENTY-CORNER-CLUSTER REFLECTOR

by

Prokopios Katris

December 1969

This document has been approved for public release and sale; its distribution is unlimited.

T133880

LIBRARY
NAVAL POSTGRADUATE SCHOOL
MONTEREY, CALIF. 93940

DUDLEY KNOX LIBRARY
NAVAL POSTGRADUATE SCHOOL
MONTEREY, CA 93943-5101

Design and Performance of a Twenty-Corner-Cluster Reflector

by

Prokopios Katris
Lieutenant, Royal Greek Navy
B.S., Naval Academy Piraeus, Greece, 1959
B.S.E.E., Naval Postgraduate School, 1968

Submitted in partial fulfillment of the
requirements for the degree of

MASTER OF SCIENCE IN ELECTRICAL ENGINEERING

from the

NAVAL POSTGRADUATE SCHOOL
December 1969

NPS ARCHIVE
1969
KATRIS, P.

ABSTRACT

This paper is a report on the design and performance of a twenty-corner-cluster (icosahedron) reflector.

Comparison of the measured cross sections of the icosahedron reflector with those of a cluster of eight corner reflectors used as a "standard" reflector shows the former being superior in performance over the latter in that it gives nearly omnidirectional response.

LIBRARY
NAVAL POSTGRADUATE SCHOOL
MONTEREY, CALIF. 93940

TABLE OF CONTENTS

LIST OF ILLUSTRATIONS

LIST OF TABLES

ACKNOWLEDGEMENT

I wish to render thanks to Professor D. B. Hoisington for suggesting the topic and for his unlimited help and advise.

I. INTRODUCTION

Radar targets are objects which scatter incident radiation from a radar such that at least a portion of it is reflected along the incident path to the antenna from which it originated. Many objects, both man-made and natural, act as radar targets. Objects such as trees, buildings, rain, clouds, birds, airplanes, ships, etc. all have been observed as radar targets. Many of these targets are not particularly effective in reflecting echoes to the radar receiver. It is possible, however, to design targets which will give much stronger echoes than most other objects of comparable size, making them very efficient reflectors. These highly efficient reflectors may be placed at appropriate points along airport runways and shipping channels to serve as "buoys" for guiding radar-equipped aircraft or ships. Alternately, they may be carried by aircraft or life rafts in order that these objects may be more readily located by ground-control crews or rescue parties. Reflectors are also used to produce standard echoes as a means of measuring radar performance.

The most familiar reflector in optics and microwave radar practice is the corner reflector. In order to extend the angular response of the single-corner reflector, clusters of several of these reflectors are often used and

the most common one is formed by three orthogonally intersecting planes.

This paper reports on the design and performance of a target reflector that will give strong specular reflection for almost any direction of incident illumination. It is a cluster of twenty triangular corner reflectors so arranged that the apertures appear like a spherical polyhedron composed of twenty triangular faces.

II. DESIGN AND PERFORMANCE OF A TWENTY-CORNER-CLUSTER REFLECTOR

A. RADAR CROSS SECTION

The study of radar targets is strongly linked with the study of electromagnetic fields scattered by these targets in an isotropic and homogeneous medium as observed at large distances from the target. The quantity of primary interest here is the distribution of electromagnetic energy far from the scattering target. For practical reasons this energy distribution is described in terms of a quantity called the radar cross section (RCS) that characterizes the scattering properties of a target.

The RCS of a target is the area normal to the incident electromagnetic wave that intersects an amount of power which when scattered equally in all directions produces an echo at the radar receiver equal to that from the target.

Mathematically this definition is expressed as:

$$\text{RCS} = \sigma = \frac{\text{power reflected/unit solid angle}}{\text{incident power density}/4\pi} \qquad \frac{\text{watts/steradian}}{\text{watts/m}^2}$$

$$\sigma = 4\pi R^2 \left| \frac{\vec{E}_r}{\vec{E}_i} \right|^2 \quad \text{meters}^2$$

where:

σ = radar cross section

R = range between radar and target

E_r = reflected field strength

E_i = incident field strength

Although the above equation is simple in form, it does not provide a means for calculating the RCS in terms of easily measured parameters. The RCS of a target depends upon radar frequency, polarization of the electromagnetic waves, aspect angle, conductivity of the reflector, surface roughness, and shape and dimensions of the reflector. Under special conditions the RCS of simply shaped targets can be calculated and expressed in terms of physical dimensions and the wavelength of the radiation, or in terms of the so-called effective area of the target. The effective area of a target is the area A of a flat plate which, when oriented perpendicular to the direction of the incident radiation, gives equal back scatter. When $A >> \lambda^2$ it is related to the RCS by:

$$\sigma = 4\pi A^2/\lambda^2.$$

Appendix A gives a table of characteristics of various types of simply shaped radar targets.

B. SINGLE TRIANGULAR-CORNER REFLECTOR

As previously mentioned the purpose of the thesis is to present the design and performance of a radar target comprised by twenty triangular-corner reflectors. For this reason the theoretical and experimental values of the radar cross section of a single corner reflector were

studied and are presented below. The results permitted the determination of the performance of the polyhedral radar reflector built and used in the experiment reported in this paper. The theoretical calculations of the RCS of a single triangular-corner reflector are based on the assumption that:

1. the conductivity of the target is infinite;

2. the target dimensions are much larger than the wave-length, so Rayleigh-region approximations may be employed;

3. the range, R, to the target is much larger than $2D^2/\lambda$ (with D the largest dimension of the target normal to the direction of radiation).

The range $R = 2D^2/\lambda$ is the far-zone criterion.

A corner reflector consists of three reflecting planes assembled so as to form a right-angle corner (Fig. 1).

If an incident ray is directed into a corner a triple reflection occurs and the ray will return in a direction parallel to and with the same polarization as the incident one. The effective area for triple reflection depends on the direction from which the corner is viewed. As the direction of the incident beam changes, the area for triple reflections gets smaller, and then double reflection occurs (from two planes whose line of intersection is normal to the line of sight), making important distributions to the effective area. Figure 2 shows a dihedral reflector and

the effects on polarization of the incident ray according to theory of reflection upon a perfectly conducting surface.

1. Calculation of the Effective Area

Consider a triangular corner reflector of edge α, with the x-axis as the axis of symmetry of the reflector and plane ABC perpendicular to the direction of the incident rays and parallel to the yz plane (Fig. 3).

When an incident ray enters the aperture or "entrance pupil" of the corner, it will, after triple reflection, appear to emerge from a point whose yz coordinates are the negative of the point of entrance. Since the aperture is defined by the surface ABC, if the negative of every point of it is plotted, the surface A'B'C' results which is called the reflected or "exit pupil." Every entering and every leaving ray will pass through the "entrance pupil." For a ray to be reflected in the same direction from which it came, it must appear to emerge from the "exit pupil" as well. Thus the effective area of a corner reflector is the area common to both the "entrance" and the "exit pupil" when projected on a plane perpendicular to the line of sight.

With the corner reflector as described in Fig. 3 and the incident rays perpendicular to ABC, the projection on YZ of the aperture remains the same, that is ABC. In Figure 4 projections of the "entrance pupil" and the "exit pupil" are shown, and the shaded area of the formed regular hexagon abcdef is their common area, or the effective area

of the reflector. Under this condition, in which the angle ϕ of the aspect is zero, the effective area is maximum.

a. Calculation of the Maximum Effective Area

Using elementary geometry and considering the symmetry of the two projected areas of Figure 4 the following relations can easily be obtained:

If α = edge of reflector = OA = OB = OC

$$AB = \sqrt{2}\alpha \tag{1}$$

$$AM = AB\cos(\pi/6) = (\sqrt{3}/2)AB = (\sqrt{3/2})\alpha \tag{2}$$

= height of ABC

$$\text{area (aAb)} = 1/2\ (ab)(Ag) = 1/2\ (AB/3)(AM/3)$$

$$= (1/6\sqrt{3})\alpha^2 \tag{3}$$

$$\text{area (abcdef)} = 6 \times \text{area (aAb)} = (1/\sqrt{3})\alpha^2 \tag{4}$$

Hence:

$$A_{max} = (1/\sqrt{3})\alpha^2 \ .$$

b. Calculation of the Effective Area for Any Aspect Angle ϕ

To find the effective area for an azimuthal angle $\phi \neq 0$, one may proceed as follows:

Consider the direction of incident rays remaining unchanged and the corner reflector turning about the point O (the center of coordinates), thus changing the aspect of viewing the aperture ABC. The task is, for an angle ϕ, to determine the yz coordinates of the A', B', and C', projections of A, B, C on the yz plane and their images A'', B'', C'' with respect to the point O. So the

"entrance pupil" and "exit pupil" are formed as projections on the yz plane and their common area can be calculated (Fig. 7).

It can be seen easily that the z coordinates for points A, B, C for any angle ϕ remain unchanged and also for their projections A', B', C'.

From Figure 4:

$$A_z = |A'_z| = (2/3)AM = ((2/3)(\sqrt{3/2})\alpha) = (\sqrt{2/3})\alpha \quad (5)$$

$$B_z = |B'_z| = C_z = |C'_z| = (1/3)AM = -(1/\sqrt{6})\alpha \quad (6)$$

For the y-coordinates consider triangle BEC as the projection of BOC on the plane x'y' (Fig. 3, Fig. 5):

$$BM = BC/2 = (\alpha/\sqrt{2}) \quad (7)$$

$$EM = \sqrt{(OM)^2 - (OE)^2} = \sqrt{\alpha^2/2 - ((1/9)(3/2)\alpha^2)}$$

$$= (1/\sqrt{3})\alpha \quad (8)$$

$$EB = \sqrt{(BM)^2 + (EM)^2} = (\sqrt{5/6})\alpha \quad (9)$$

In Figure 6 the triangle BEC (solid lines) is turned by an angle ϕ (the aspect angle) on its new position BEC (dotted lines). The projections B', M', C' on the y'-axis will be calculated as a function of ϕ:

$$|A'_y| = EM' = EM\sin\phi = (1/\sqrt{3})(\sin\phi)\alpha \quad (10)$$

$$B'_y = -EB' = -EB\sin(\phi'+\phi)\alpha$$

$$= -(\sqrt{5/6})((\sin(\phi'+\phi))\alpha \quad (11)$$

$$C'_y = EC\sin(\phi'-\phi) = (\sqrt{5/6})(\sin(\phi'-\phi))\alpha \qquad (12)$$

with $\tan\phi' = BM/EM = (\alpha/\sqrt{2})/(\alpha/\sqrt{3}) = \sqrt{3/2}$:

$$\phi' = 50.77^\circ$$

From the trigonometric identity:

$\sin(\phi'\pm\phi) = \sin\phi'\cos\phi \pm \cos\phi'\sin\phi$, and since

$\sin\phi' = BM/EB = (1/\sqrt{2})/(\sqrt{5/6}) = \sqrt{3/5}$,

$\cos\phi' = EM/EB = (1/\sqrt{3})/(\sqrt{5/6}) = \sqrt{2/5}$:

$$|A'_y| = (1/\sqrt{3})(\sin\phi)\alpha \qquad (10)$$

$$B'_y = -((1/\sqrt{2})\cos\phi + (1/\sqrt{3})\sin\phi)\alpha \qquad (13)$$

$$C'_y = ((1/\sqrt{2})\cos\phi - (1/\sqrt{3})\sin\phi)\alpha \qquad (14)$$

$$A'_z = (2/\sqrt{6})\alpha \qquad (5)$$

$$B'_z = C'_z = -(1/\sqrt{6})\alpha. \qquad (6)$$

The above set of equations determines the projection A'B'C' on the yz plane and its image A''B''C'' with respect to O.

Figure 7 shows such a projection and the effective area. It can be seen how this area changes with angle ϕ by comparison with Figure 4.

Table I gives the values of the effective areas and the corresponding angles, while Figure 8 is a plot of these values vs ϕ.

c. Calculation of the Effective Area of the Dihedral Reflector

When the aspect angle is $\phi = \pi/2 - \phi' = 39.23°$ the RCS due to bihedral reflection becomes zero (Table I, Fig. 8). In this position of the reflector where EB lies on the y'-axis (Figs. 9 and 10) the entrance pupil and exit pupil do not have any common area and triple reflection vanishes. In this position also triangle OEB (Fig. 3) lies in the yz plane as does line segment OB; but OB is the intersection of the perpendicular planes OAB and OBC which form the dihedral reflector. Alternately the condition for dihedral reflection along the same path as the incident beam is that the intersection OB of the dihedral must be normal to the line of sight, and this condition is satisfied since the incident rays remain perpendicular to the yz plane. The planes of incidence, where the "plane of incidence" is defined as the plane formed by the incident ray and the vector normal to the surface of the reflector, will be perpendicular to OB and consequently parallel to plane OAC, while their intersections with plane x'y' or xy will be lines parallel to the x' or x-axis, that is, to the direction of the incident radiations. In Figure 9 is shown the projection of the corner reflector on the plane yz with line segment A'OC' defined by the projection of points A, O, C and with line 11' representing the intersection with a plane of incidence.

Figure 10 is the projection of the reflector on the x'y' plane where line mm' is the intersection with plane OAC while line ll' is the intersection with another plane of incidence. In the same figure point G is the point where the extention of line segment OA meets the plane x'y'. The so formed right-angle triangle OCG has one side equal to OC = α (side of the reflector) and the hypotenuse:

$$CG = MC/\cos\phi' = (\alpha/\sqrt{2})(\sqrt{5/2}) = (\sqrt{5}/2)\alpha \qquad (15)$$

The following relations are also obvious:

$$OG = \sqrt{(CG)^2 - (OC)^2} = \alpha/2 \qquad (16)$$

$$\cos(O\hat{C}G) = OC/CG = \alpha/((\sqrt{5}/2)\alpha) = 2/\sqrt{5} \qquad (17)$$

$$\sin(O\hat{C}G) = OG/CG = (\alpha/2)/((\sqrt{5}/2)\alpha) = 1/\sqrt{5}$$

The angle $O\hat{C}G$ is of importance for the calculation of the effective area because it is equal to the angle of incidence. The planes of incidence are infinite in number starting from point B, with the outermost being the plane OAC.

Figure 11 shows this plane with B = OCG = angle of incidence, and also paths followed by incident rays. All rays striking the reflector on their way back reach the line segment CK in phase since it is easy to prove that their paths are equal. The CK segment lies on the plane of incidence and is perpendicular to the incident rays having a length defined as follows:

$$CF = OC/\cos\beta = \alpha/(2/\sqrt{5}) = (\sqrt{5}/2)\alpha \quad (19)$$

(from triangle OCF and using Eq.(17))

$$CK = CF\sin 2\beta = 2CF\cos\beta\sin\beta = (2/\sqrt{5})\alpha \quad (20)$$

Any rays not entering and leaving the reflector through segment CK are lost without returning to the receiver.

The projection of CK on the yz plane (Fig. 9) will lie on line A'OC' in such a way that C'K' = CK and the point C' and K' will be symmetric with respect to point 0.

The area of the triangle BC'K' is the area under which double reflection occurs, while the rest of the yz projection (area A'BK') does not contribute to the effective area. The effective area of the dihedral thus is:

$$A_d = (1/2)(OB)(C'K') = (1/2)(OB)(CK) = (1/\sqrt{5})\alpha^2 \quad (21)$$

For $\alpha = 3.364''$ and $\lambda = 3.33 \times 10^{-2}$ m:

$$\sigma = (4\pi/\lambda^2)A_d^2 = 1.552 \text{ m}^2. \quad (22)$$

Equation (22) does not represent a true value for the case where the incident electromagnetic radiation is, let's say, vertically polarized and with the receiver polarized in the same way. Under this assumption and since the plane of incidence makes an angle with the vertical the polarization of the reflected radiation will describe also a certain angle with the vertical direction (direction of receiver polarization).

According to another expression for the RCS:

$$\sigma = (4\pi R^2)|\vec{E}_r \cdot \vec{p}/\vec{E}_i|^2 = (4\pi R^2)|\vec{E}_r/\vec{E}_i|^2 \cos^2\psi \quad [1]$$

$$= (4\pi/\lambda^2) A_d^2 \cos^2\psi \quad (23)$$

where $\vec{p}$ is a unit vector denoting the receiver polarization.

To find ψ, consider the components of the incident field $\vec{E}_i$, one on the plane of incidence and the other on a plane perpendicular to it (Fig. 12). The first component, undergoing double reflection, appears to emerge from the reflector with a phase shift of 180° while the latter is reflected unchanged. Figure 12 is the schematic diagram of the vector fields just described. Under the assumption that reflection takes place on perfectly conducting plates, $\vec{E}_r$ is the conjugate vector of $\vec{E}_i$ having a different phase, $\pi + \psi$. It is also obvious that ψ is twice the angle between the plane of incidence and the incident field $\vec{E}_i$. The latter, according to Figure 9, is equal to OBC' = $\psi/2$.

From triangle OBC' (Fig. 9):

$$\cos \psi/2 = \cos(OBC') = OB/BC' = \alpha/((\sqrt{6/5})\alpha) = \sqrt{5/6} \quad (24)$$

$$\cos\psi = 2\cos^2(\psi/2) - 1 = 10/6 - 1 = 2/3 \quad (25)$$

Equation (22) is then finally written as:

$$\sigma = (4\pi/\lambda^2)\ A_d^2 \cos^2\psi = 1.552(2/3)^2 = .69\ m^2. \quad (22)$$

d. Experimental Measurements

The corner reflector's RCS was measured in an indoor anechoic chamber using a FM/CW transmitter-receiver setup discussed in the following chapter. The RCS was plotted on an x-y recorder, scaled, and replotted on Figure 8 for comparison with the theoretical values. The experimental results appear to be very satisfactory. Small differences exist at the peak value of the triple reflection region with the measured RCS 0.48-db higher than the calculated value, while for an azimuth angle ϕ of 10 to 15° the calculated RCS exceeds the measured one by at most 0.5 db. In the region of double reflection the experimental curve appears as was expected, not having sharp peaks at both ends of the triple reflection region but having a finite beam-width. At one of these peaks the difference between the two plots is 1.9 db which is the greatest difference, while for the other peak this difference is only 0.4 db. The above differences can be considered to be well within experimental accuracy.

C. EXPERIMENTAL METHOD FOR MEASURING THE RADAR CROSS SECTION

1. General

Radar targets in general are of very complex shape and have non-uniform electrical parameters so that the theoretical formulas for the scattering cross section cannot be used (exceptions are the cases involving simple objects, i.e. a corner reflector). For this reason one

must obtain backscattering cross sections by measurements, and measuring techniques of good accuracy and sensitivity need to be developed. In recent years several methods based on new principles have been developed to measure the radar cross section. Some of the representative methods are the following:

- Standing-wave method
- Doppler-shift method
- Magic-T method (or cw balanced-bridge method)
- Space-separation method
- Time-separation method
- FM/CW radar method.

All of these experimental methods of measuring the RCS have advantages and disadvantages. In particular, the FM/CW radar method, which was the one used for the experimental measurements of the targets discussed in this paper has the following features: it is superior to other methods in the fact that the influence of the wave scattered from the background is reduced appreciably. This is achieved by adopting a highly selective amplifier in the FM radar. On the other hand, in this method the backscattering cross section at a specific frequency cannot be measured accurately because of the deviation of the frequency used in measurement. However, the frequency deviation has only a slight influence since it is much smaller than the frequency in question. The ability to measure larger targets has been somewhat limited also since a very small change in

frequency results in a relatively large phase shift making the RCS measurement erroneous.

2. Measuring Device

A block diagram of the measuring setup is shown in Figure 13. The setup consists of

1. FM transmitter: The ALFRED 605 microwave oscillator utilizing a backward-wave-oscillator tube was used as the FM transmitter. The characteristics of the oscillator usable for the experiment are:

Power output 10 mw min (15mw used)

Frequency range 1 to 26.5 GHz

Sweep: recurrent sweep due to an internal sawtooth voltage scanning repetitively the frequency of the rf signal, linearly from low to high over the range selected and bound by dial settings. Sweep period 10 msec with corresponding repetition frequency f_r = 100 repetitions/sec.

2. Isolator: A ferrite isolator having negligible forward loss and providing about 50-db attenuation for the received signal is used after the oscillator; that is, the oscillator is effectively decoupled from the load.

3. Frequency meter

4. Hybird-T junction: A four-port microwave junction isolates the transmitted and received signals permitting a moderate amount of leakage to enter the receiver along with the echo signal so that the latter can be heterodyned in the non-linear crystal mixer to produce a beat frequency.

5. Tuner: For matching purposes

6. Rectangular horn antenna

7. Crystal mixer: The element that combines the outgoing frequency with the incoming frequency to produce the beat note (difference frequency). This beat note is a measure of the target's range, while the amplitude of the beat note is proportional to the RCS of the target and also the principal item of interest in the experiment.

8. Receiver amplifier: HP-465 A audio amplifier

9. Full-wave bridge rectifier with capacitor filter

10. X-Y recorder: To plot the rectified received signal scaled in meters^2 of the RCS.

3. Characteristics of the System

The carrier frequency used in the measurements was f_o = 9 GHz and the deviation $\Delta f \approx 60$ MHz.

In Figure 14a the sawtooth voltage which modulates the carrier frequency is shown. The positive slope of this waveform causes a linear increase of the output frequency from f_o to $f_o + \Delta f$. Upon arrival at the uppermost frequency rapid retrace occurs. The output frequency remains at its starting value, f_o, until the sweep is initiated again.

In Figure 14b the solid curve represents the transmitted frequency-modulated signal; the dashed curve represents the echo returning from the target at distance R after time T = 2R/c, where c is the velocity of

propagation. If $\Delta f/\Delta t$ is the rate of change of the carrier frequency, the beat frequency, f_b, is:

$$f_b = (\frac{\Delta f}{\Delta t})T = \frac{2R}{c}\frac{\Delta f}{T_r-\tau'} \quad \text{for } nT_r + T \leq t \leq (n+1)T_r - \tau'$$

where:

T_r = sweep period = 10 msec

τ' = retrace time = 1.8 msec

with distance between target and horn antenna equal to R = 4.7m, so that

$$f_b = \frac{2 \times 4.7 \times 60 \times 10^6}{8.2 \times 10^{-3} \times 3 \times 10^8} = 229 \text{ Hz.}$$

For the interval $(nT_r - \tau') < t < (nT_r + T)$ the beat frequency is many orders of magnitude larger. These frequency components, since they are filtered out at the receiving stage, will be omitted in the following analysis and the wave form after the crystal mixer will be assumed to be as in Figure 14d.

This waveform will be treated as a pulsed sine-wave with repetition period T_r and pulse duration $\tau = T_r - T - \tau'$, and the frequency spectrum will be determined.

Choosing the time origin as in Figure 14d the mathematical expression as a function of time is:

$$f(t) = 0 \quad \text{for } -T_r/2 \leq t < -\tau/2,$$

$$\tau/2 < t \leq T_r/2$$

$$f(t) = V_o \cos\omega_b t \qquad -\tau/2 \leq t \leq \tau/2$$

The Fourier complex coefficients C_n are:

$$C_n = \frac{1}{T_r}\int_{-\tau/2}^{\tau/2} f(t)e^{-jn\omega_r t}\,dt = \frac{V_o}{T_r}\int_{-\tau/2}^{\tau/2} \cos\omega_b t\, e^{-jn\omega_r t}\,dt$$

$$= \frac{V_o}{2T_r}\left[\frac{e^{j(n\omega_r-\omega_b)\tau/2} - e^{-j(n\omega_r-\omega_b)\tau/2}}{j(n\omega_r-\omega_b)} + \right.$$

$$\left.\frac{e^{j(n\omega_r+\omega_b)\tau/2} - e^{-j(n\omega_r+\omega_b)\tau/2}}{j(n\omega_r+\omega_b)}\right]$$

$$= \frac{V_o\tau}{2T_r}\left[\frac{\sin(n\omega_r-\omega_b)\tau/2}{(n\omega_r-\omega_b)\,/2} + \frac{\sin(n\omega_r+\omega_b)\tau/2}{(n\omega_r+\omega_b)\tau/2}\right] \qquad (26)$$

Equation (26) defines the frequency spectrum which is shown in Figure 15. The spectrum has a sin x/x shape centered around the frequency f_b in which the maximum value of amplitude equals $V_o\tau/2T_r$. This maximum value depends on R, since:

$$V_o\tau/2T_r = V_o(T_r - \tau')/2T_r - V_oT/2T_r$$

$$= V_o(T_r - \tau')/2T_r - (V_o/2T_r)(2R/c). \qquad (27)$$

The first term of equation (27) depends entirely upon the transmitter-receiver's constants, while the second term is a function of the target range. However, since the experiment took place in an indoor anechoic chamber and the range between antenna and reflector was limited to 4.7

meters, this term is negligible being much smaller than the first one.

The frequency spectral analysis completed above points to the desirability of a narrow-band amplifier for the reception stage, centered at the frequency f_b = 230 Hz. Thus, the echo from the walls and any obstacles existing behind or closer to the reflector under measurement will be eliminated. Although the amplifier used for the setup does not employ the required narrow frequency band, this fact did not affect the accuracy of the measurements taken because of the non-reflecting background used. The experimental measurements on the corner reflector's RCS and the comparison of them with the theoretical values verifies the good performance of the transceiver setup.

4. Anechoic Chamber

The experiment took place in a room whose dimensions are shown in Figure 16. The walls, ceiling and floor are covered by absorbing material to create a non-reflecting environment. The absorbing material consists of mats of curled animal hair impregnated with a mixture of graphite in a rubber solution giving 15-20 db absorption. A turntable, controlled from an outside control room, was isolated from the antenna's view by a thick wall of the above absorbing material placed in front of the turntable in such a way as to cover everything but the reflectors placed on it. The separation between the horn antenna of the setup and the reflector under measurement was kept at R = 4.7 m, while

both were placed at the same height above the floor, namely 1.15 m.

The beamwidth of the radiation pattern for the horn antenna used was 11.3° and 11.65° in the vertical and horizontal planes respectively, approximately corresponding to a rectangular surface of about 0.955-m width and 0.92-m height centered at the target's position. Thus, considering the dimensions of the room (Fig. 16), it can be seen that reflections from the side walls or floor were avoided, and reflections from the wall behind the target that could contribute to the echo, were limited by the absorbing material and also by the fact that this wall made an noticeable angle with respect to the angle of the radiation.

D. THE TWENTY-CORNER-CLUSTER REFLECTOR

1. Description

The twenty-corner-cluster reflector is a reflector whose aperture is a regular icosahedron (solid figure with twenty plane surfaces) with each plane surface equal to the equilateral triangular aperture of the single corner reflector. The advantage of this reflector is that it gives relatively strong echoes from any direction of illumination. It has nearly full response over 360° in azimuth and ±90° in elevation for linearly polarized radiation (assuming that the receiving antenna has the same polarization as the transmitting antenna).

Figure 17 is a picture of the reflector, while Figures 18 and 19 describe its geometry.

When the reflector is observed in the direction of an axis of symmetry (axis passing through the center of its body and two vertices) a cluster of five corners appears in view. Figure 18 is a projection of the reflector on a plane vertical to this axis of symmetry. The regular pentagon BCDEF, formed by five vertices of the icosahedron has sides of length $\sqrt{2}\alpha$ and can be inscribed into a circle of radius $R = BC/1.176 = \sqrt{2}\alpha/1.176$. Points G,K,L,M,N are also vertices of a similar pentagon which can be viewed from a direction opposite to the axis of symmetry. In the same figure the points b, c, d, e, f are the vertices of the single-corner reflectors in view, and they form a regular pentagon inscribed in a circle of radius $R=0.21\alpha$.

Figure 19 is an intersection of the reflector with a vertical plane passing through vertices A, B, L (Fig. 18).

2. RCS Measurements of the Icosahedron Reflector

Radar cross section measurements are almost always relative in that the cross section from the body under test is compared with the cross section of a "standard" body.

As the standard reflector a cluster of eight corner reflectors was used (Fig. 20). The corner reflectors of the standard had the same dimensions as had the corner reflectors of the icosahedron under test. With the incident ray continuously directed to the target under test (the

direction was the horizontal line joining the antenna and the center of the target) each reflector was successively positioned on the turntable and supported in such a way that it could be rotated about the vertical axis.

Rotation about the horizontal axis was performed step by step by changing the elevation angle, θ, in two-degree steps for the range - 90° to + 90°, while for each angle of elevation a full rotation about the vertical axis was performed changing the azimuth angle, ϕ, continuously from 0° to 360°. Two complete sets of patterns were obtained describing the scattered radiation intensity of the reflectors. They were scaled in square meters of cross section, σ, using for calibration square flat plates of known σ.

A total of 22 patterns was required for the standard reflector because of the rotational symmetry of the body, and 45 patterns for the icosahedron reflector. Figures 21 to 24 are samples of these patterns representing the eight-corner cluster, and in particular for $\sigma(\phi,\theta = 0)$, $\sigma(\phi,\theta = 4°)$, $\sigma(\phi,\theta = 12°)$, and $\sigma(\phi,\theta = 45°)$.

Figure 21, or $\sigma(\phi,\theta = 0\ )$, is the pattern corresponding to the optimum position of this reflector with respect to the incident beam. In this position two of its three planes (namely the plates ACDF and ABDE of Fig. 20) are vertical, and as the reflector rotates about its vertical axis they face the incident beam at right angles and in intervals of 90° in the azimuth range ϕ, offering the

maximum RCS. This fact creates the five sharp peaks in Figure 21 (the fifth being the repetition of the first), while the pattern between these peaks shows the cross section due to the contribution of the dihedrals formed by the vertical plates. As the elevation angle θ changes, the cross section changes rapidly. The plate ACDF (Fig. 20) being perpendicular to the horizontal axis of rotation remains vertical for all θ producing sharp peaks every 180° of azimuth angle. These peaks should be observed in all patterns with equal magnitude; however they do not, and this is due to the fact that even a slight deviation from the perpendicular position of a flat plate with respect to the incident rays is enough for the echo to vanish, especially when the receiving antenna has a very narrow pattern.

In Figure 24 the sharp peaks have a small magnitude for the above reason. The dotted line represents the theoretical pattern.

Figures 25 through 28 are patterns taken from the icosahedral reflector and give the impression of a randomly varying cross section. This is primarily due to the fact that energy is being reflected from more than one corner, and that these radiations add with changing relative phase as the angle changes. It is obvious that the icosahedral reflector gives large cross sections from almost any aspect of incident radiation, appearing superior to the eight-corner cluster used as a comparison standard.

A statistical comparison was made between the icosahedral reflector and the eight-corner reflector as described in the following section.

3. Statistical Evaluation

The remaining task is to define the statistics of the two sets of data taken which will enable one to compare the two reflectors. More specifically, the cumulative distributions of the two sets will be considered and a direct comparison made between the two.

The available data representing the variations of the RCS of the designed reflector and the "standard" one are continuous with respect to azimuth angle ϕ and discrete with respect to elevation angle θ (taken every two degrees).

Dividing the ϕ-domain of each pattern every two degrees and taking the average value of this interval, samples of cross section σ are obtained, corresponding to small elements of known solid angle. 8280 samples were obtained for the icosahedron reflector covering the total ϕ and θ-domains corresponding to 4π solid radians, while 4140 samples were obtained for the "standard" reflector. These data were grouped in intervals for every one-half square meter of cross section σ and the solid angle related to these intervals was computed.

Histograms of the solid angle for intervals of σ covering a range from 0 to 14 m^2 are shown in Figures 29 and 30 for both reflectors. The ordinate of these figures was normalized; the normalization factor is 4π. The

normalized histograms are an estimate of the probability density function, $p(\sigma)$.

Figures 31 and 32 are the cumulative distributions derived from the histograms and represent the probability that the RCS σ will be less than a defined value σ_o, $P(\sigma<\sigma_o)$.

For comparison between the two reflectors Figure 33 shows plots of the functions $P(\sigma_o<\sigma) = 1 - P(\sigma<\sigma_o)$, that is, the probability that the cross section σ exceeds the value σ_o.

From Figure 33 the superiority of the newly designed icosahedral reflector in comparison with the "standard" eight-corner-cluster reflector is obvious, since for any σ_o the former reflector has higher probability of exceeding the value σ_o than has the latter one.

Tables II and III contain the data plotted in Figures 29, 30, 31, and 32. Column 2 is the probability density corresponding to the interval boundaries numbered in column 1, and column 3 shows the related cumulative distribution values for these boundaries.

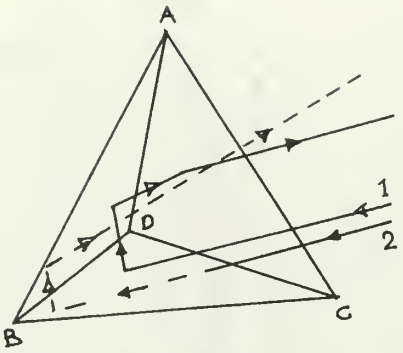

Figure 1. Corner reflector showing ray paths. Ray 1 undergoes three reflections while ray 2 undergoes two reflections and goes off at an angle oblique to the incident ray.

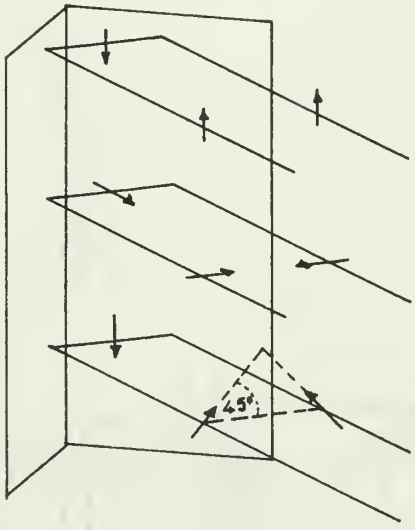

Figure 2. Dihedral reflector and polarization effect. When the incident ray is polarized parallel or perpendicular to the line of intersection of the two surfaces the reflected ray is polarized in the same plane as the incident ray. If the incident ray is polarized at a different angle the reflected ray will have different polarization and will not ordinarily be accepted by the same antenna from which the incident radiation was launched.

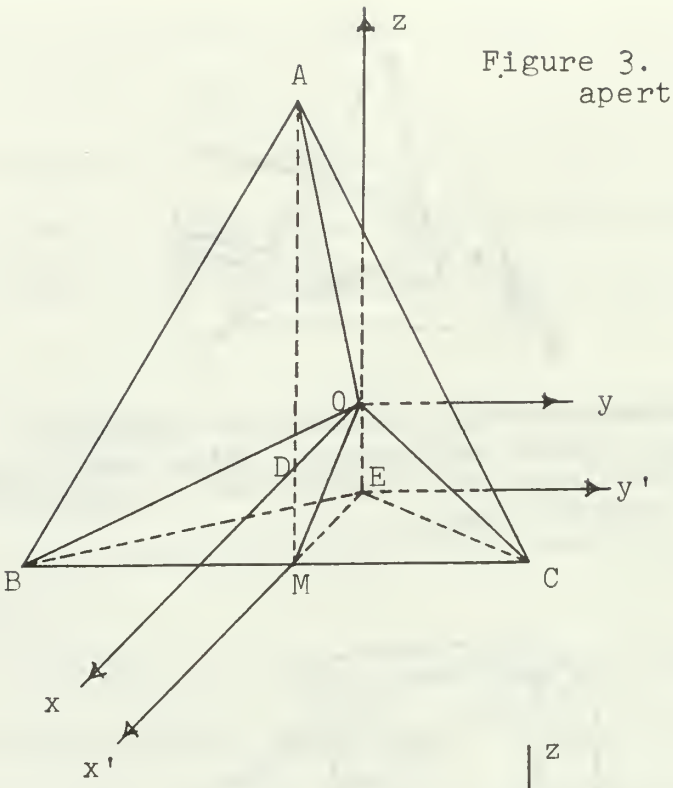

Figure 3. Corner reflector, aperture plane vertical

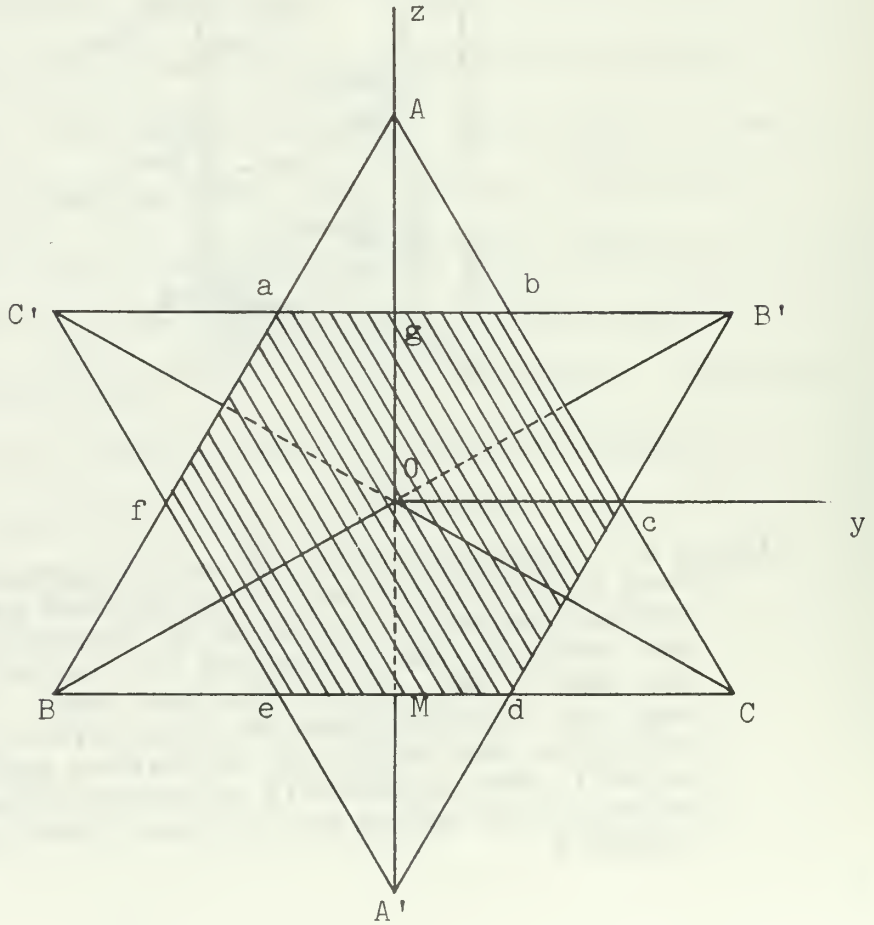

Figure 4. Maximum effective area of corner reflector, projection on xz plane

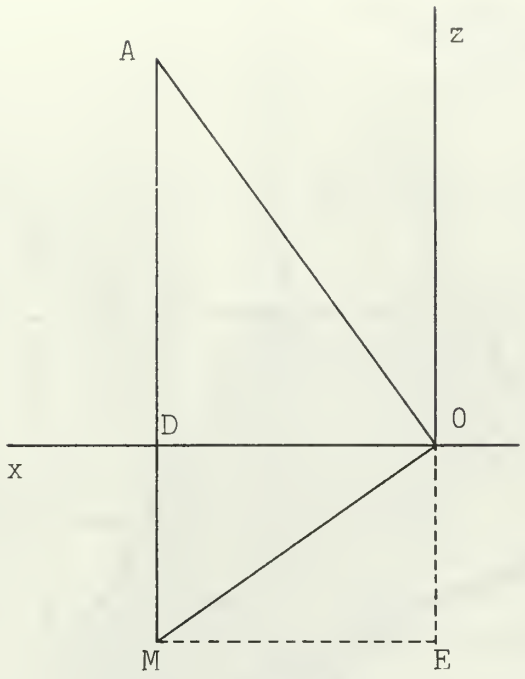

Figure 5. Corner reflector, median plane

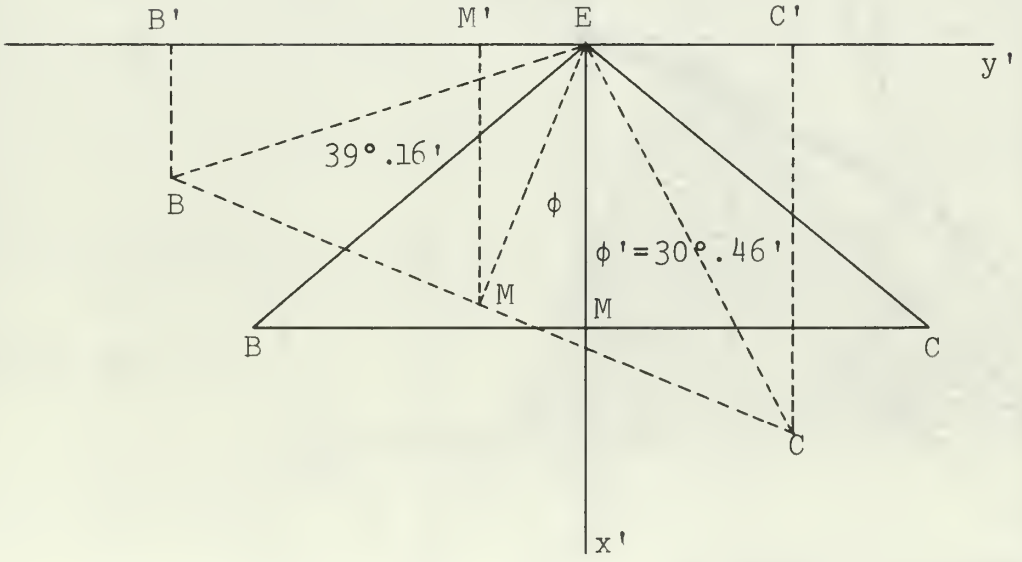

Figure 6. Corner reflector, x'y'-projection

Figure 7. Corner reflector, effective area with aspect angle $\phi \neq 0$

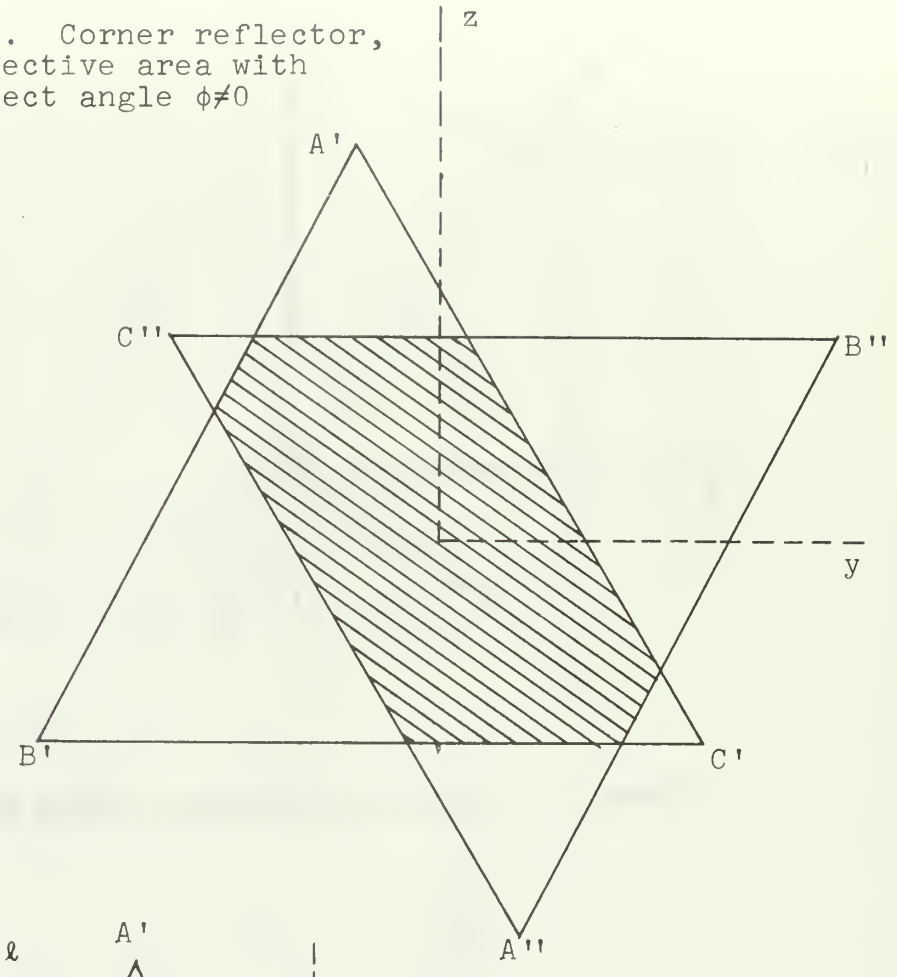

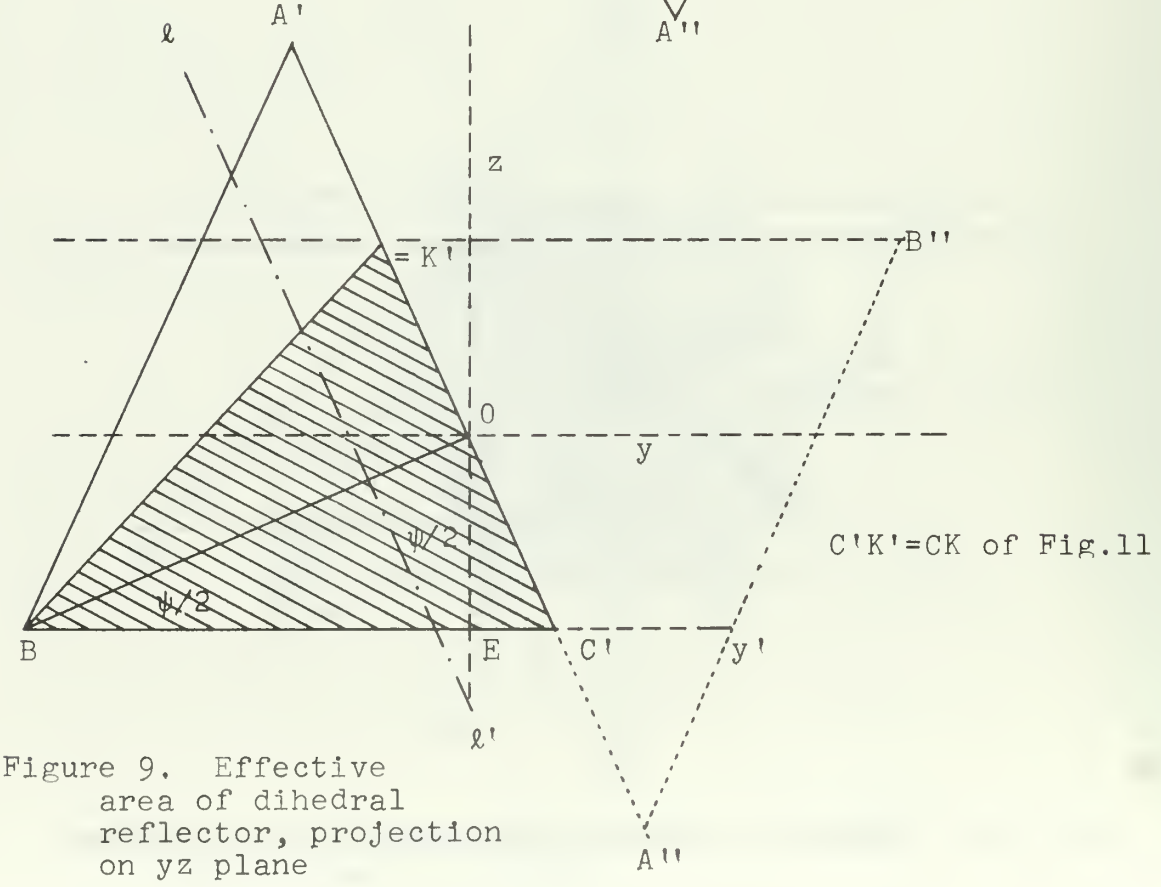

Figure 9. Effective area of dihedral reflector, projection on yz plane

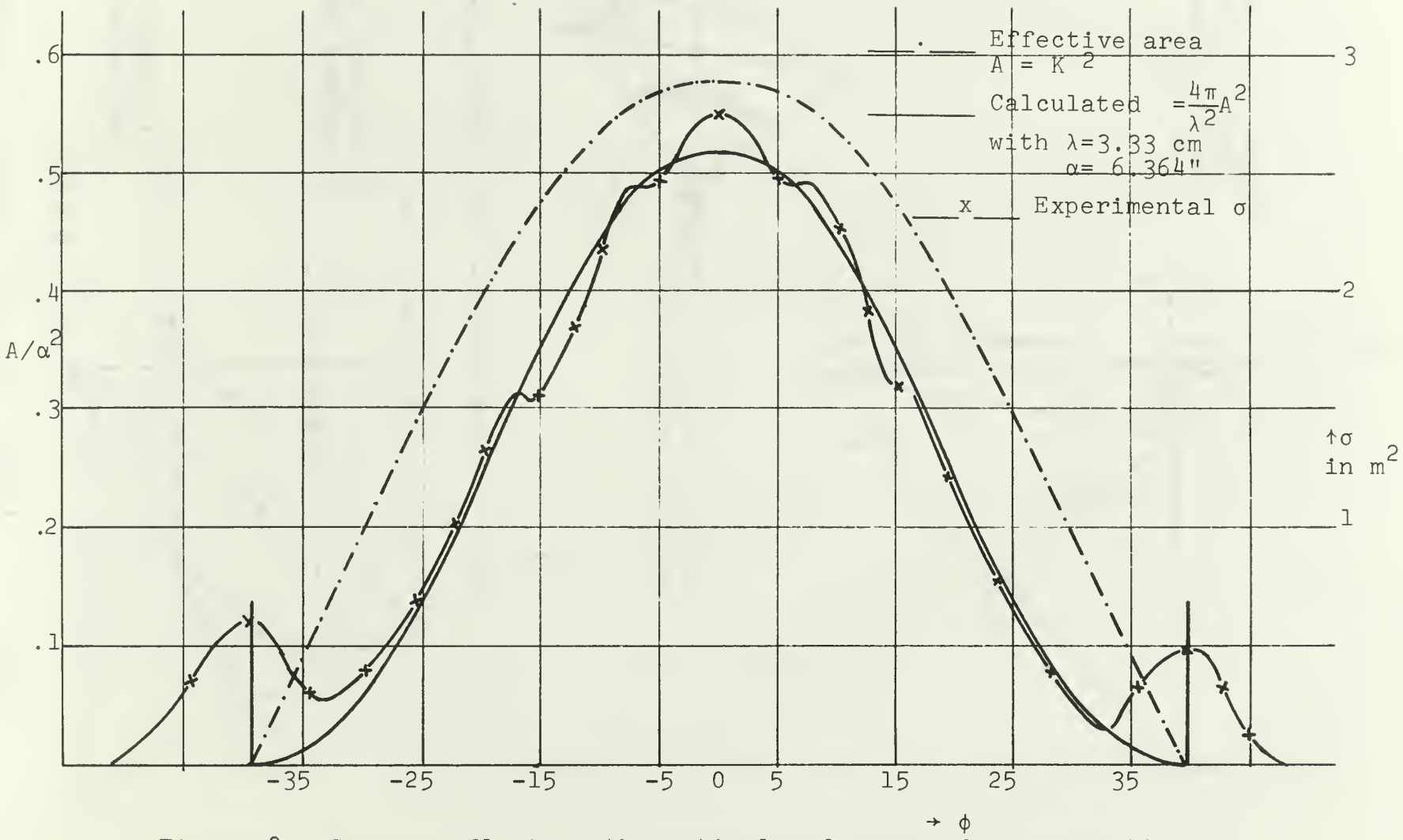

Figure 8. Corner reflector, theoretical and measured cross sections

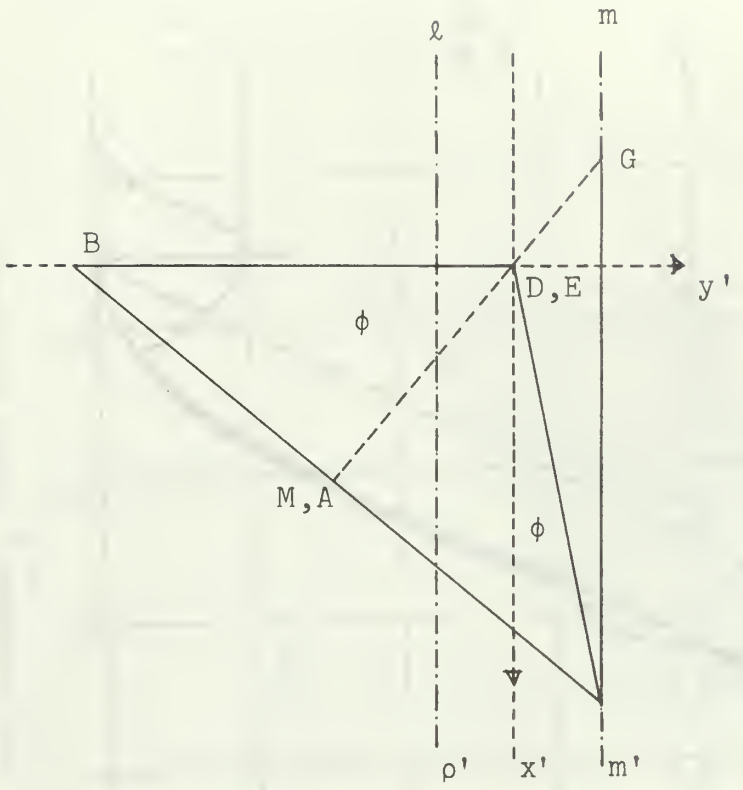

Figure 10. Corner reflector, projection on x'y' plane for $\phi = 39.23°$

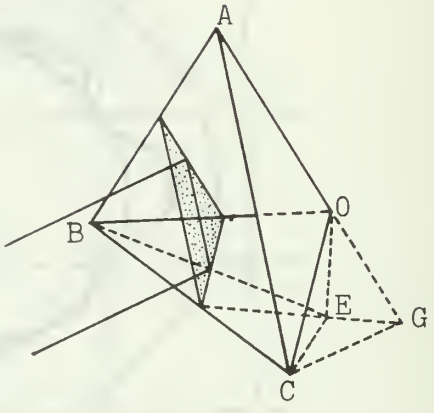

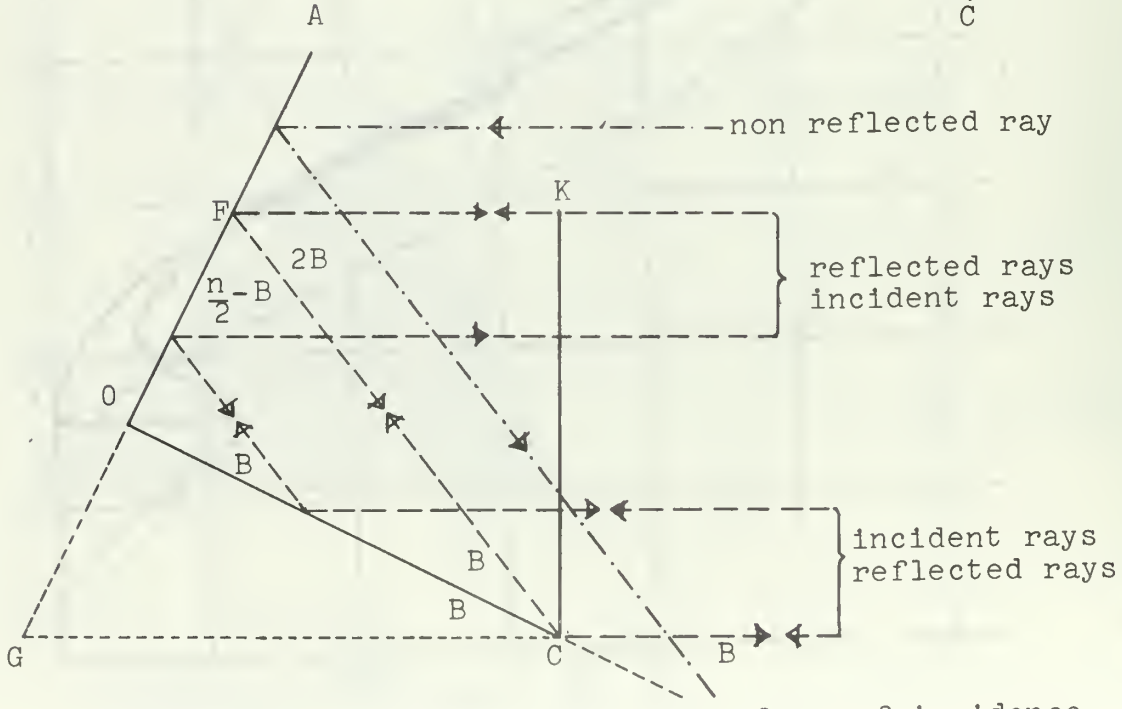

Figure 11. Dihedral reflector, plane of incidence

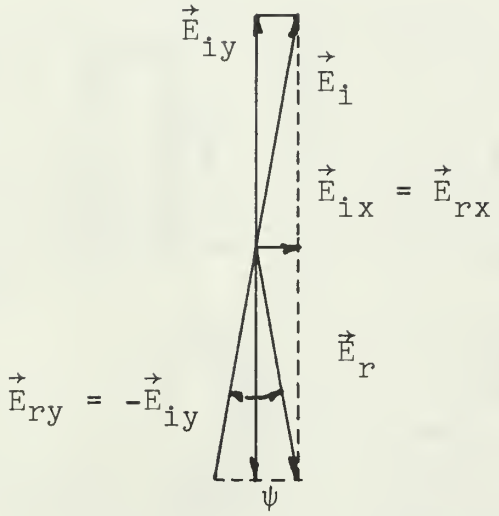

Figure 12. Diagram showing polarization angle, ψ

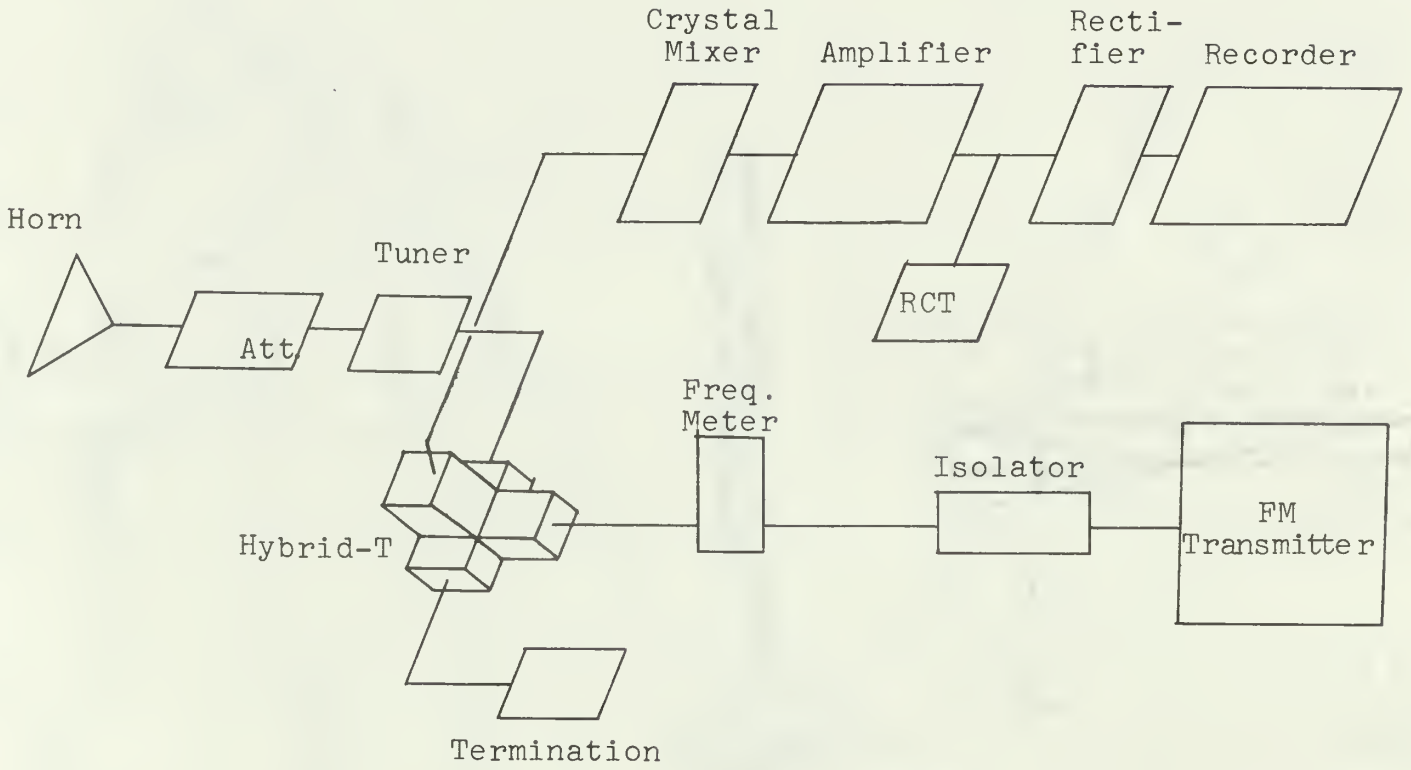

Figure 13. Diagram of experimental setup

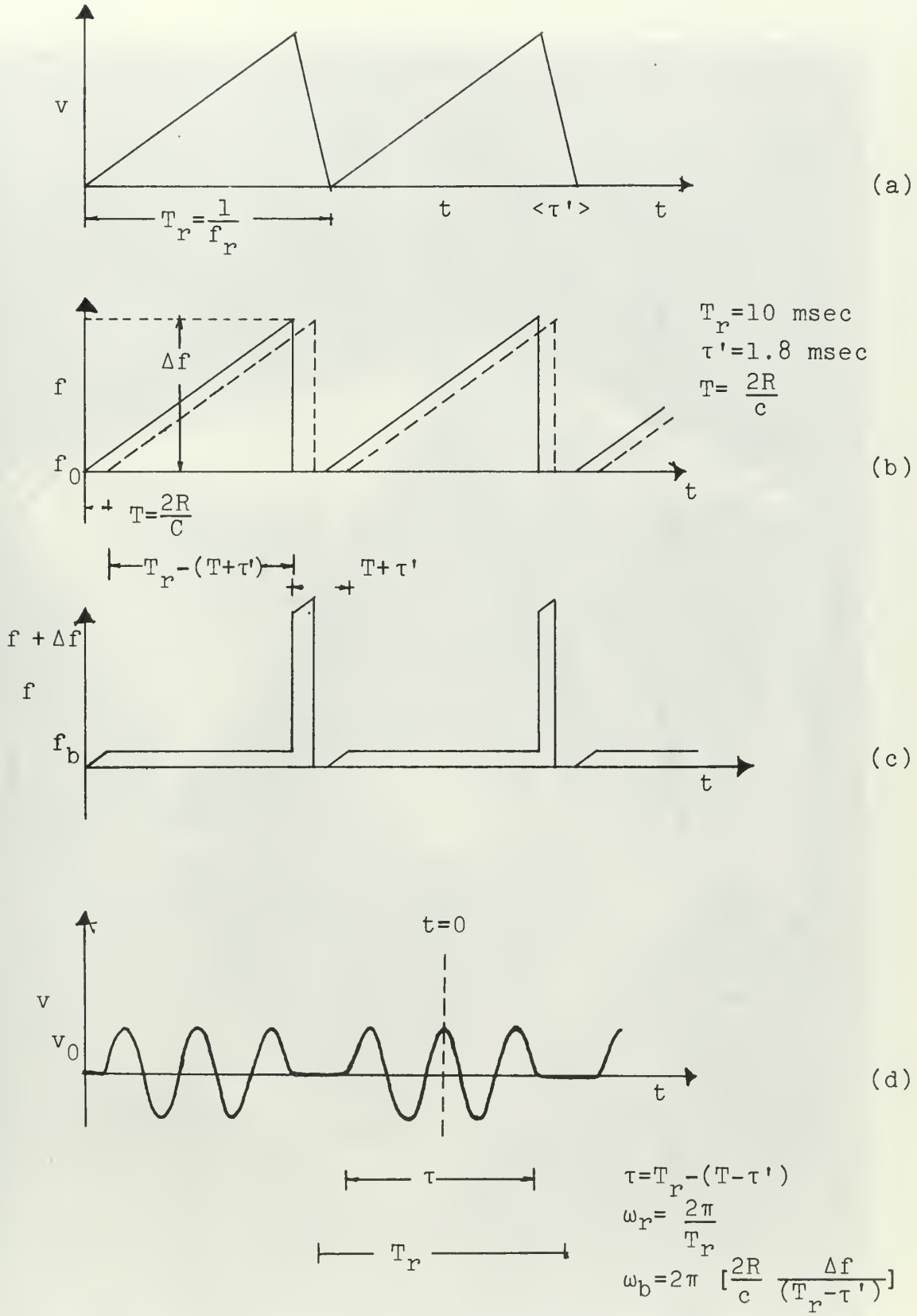

Figure 14. Frequency-time relationship in the FM/CW setup

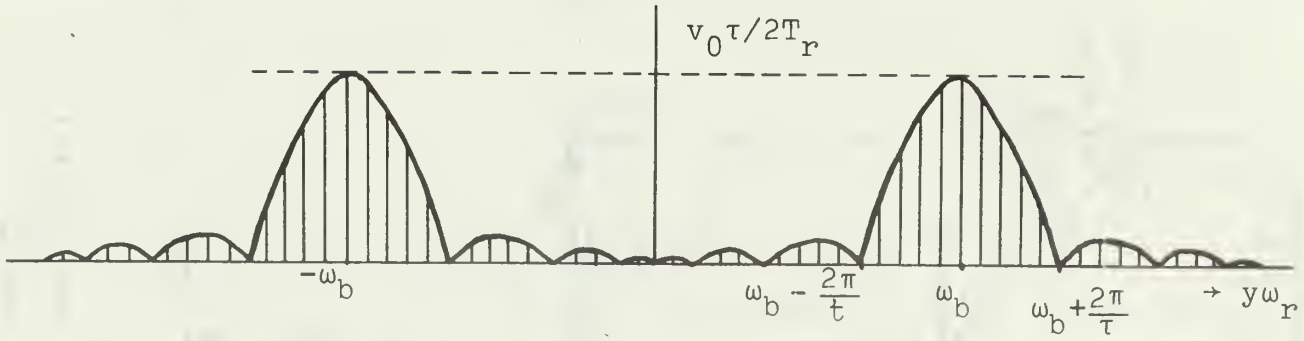

Figure 15. Frequency spectrum

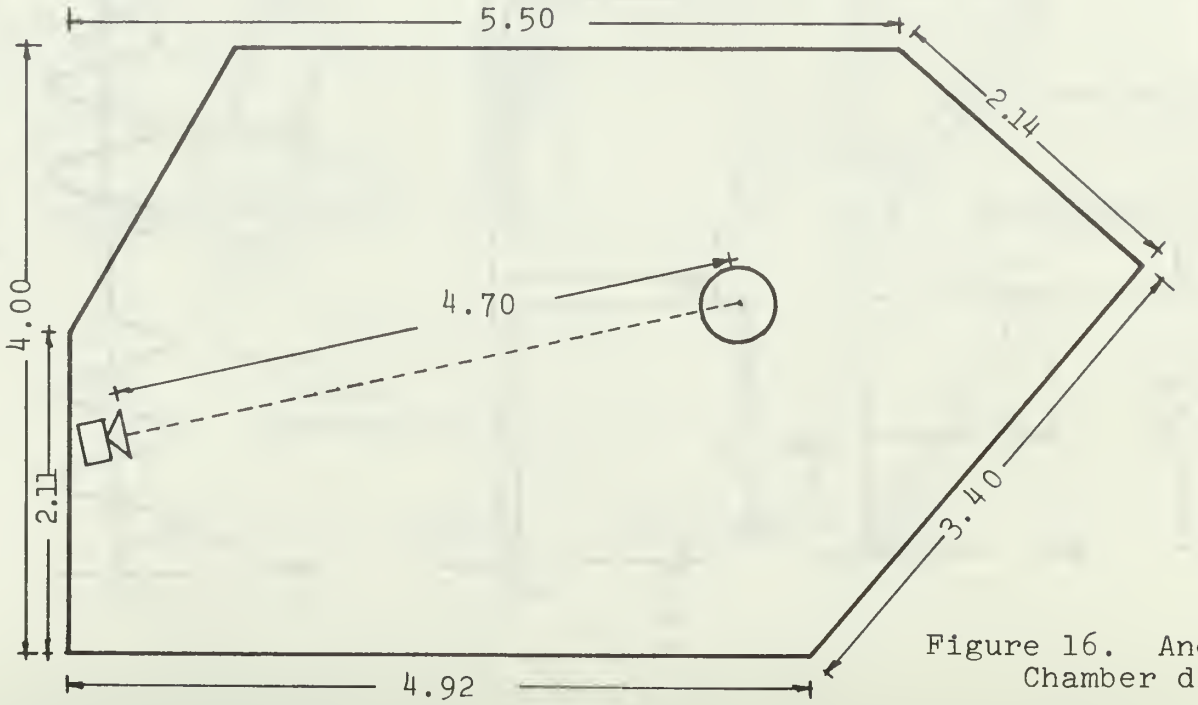

Figure 16. Anecoic Chamber diagram

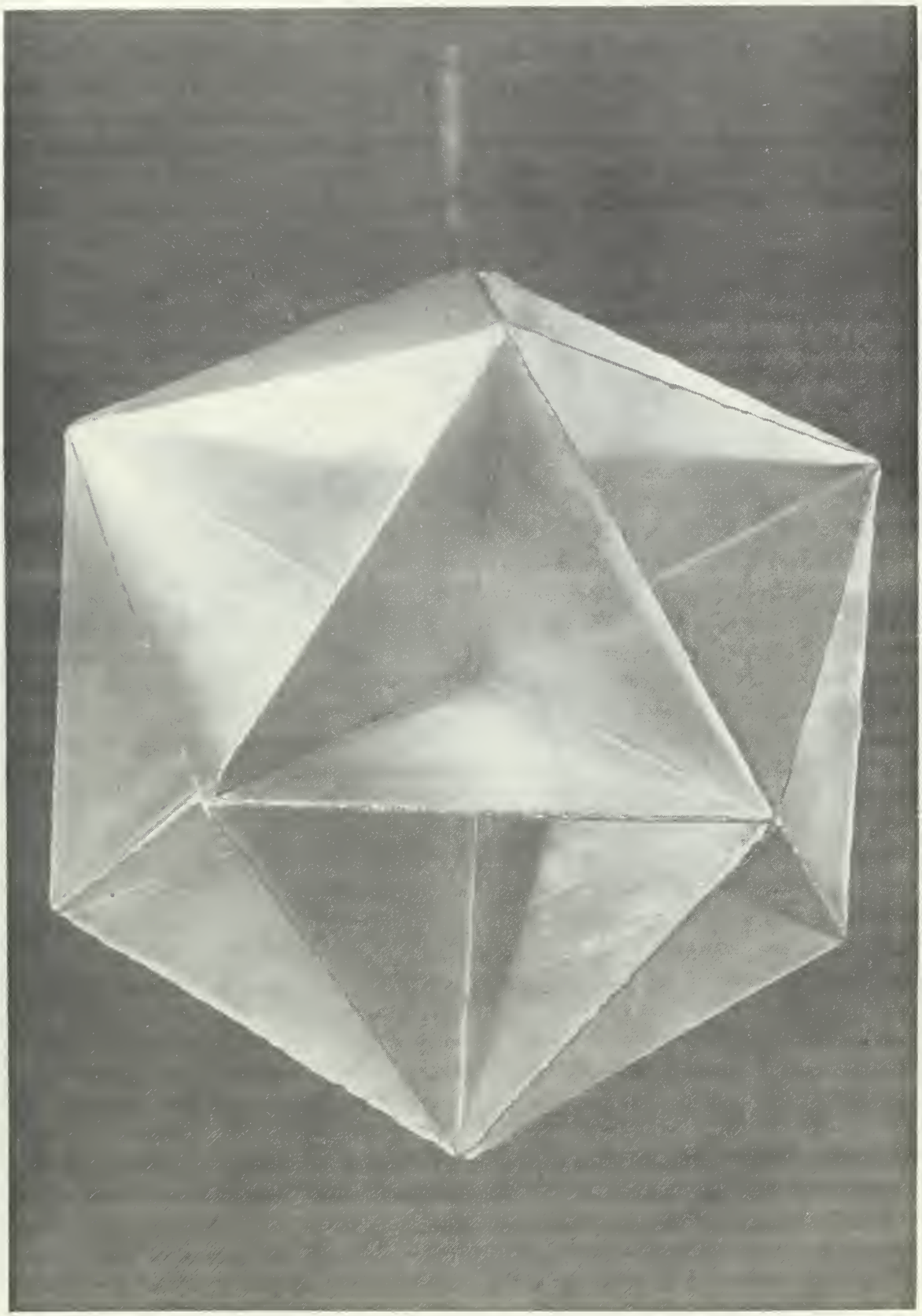

Figure 17. Photograph of the icosahedral reflector

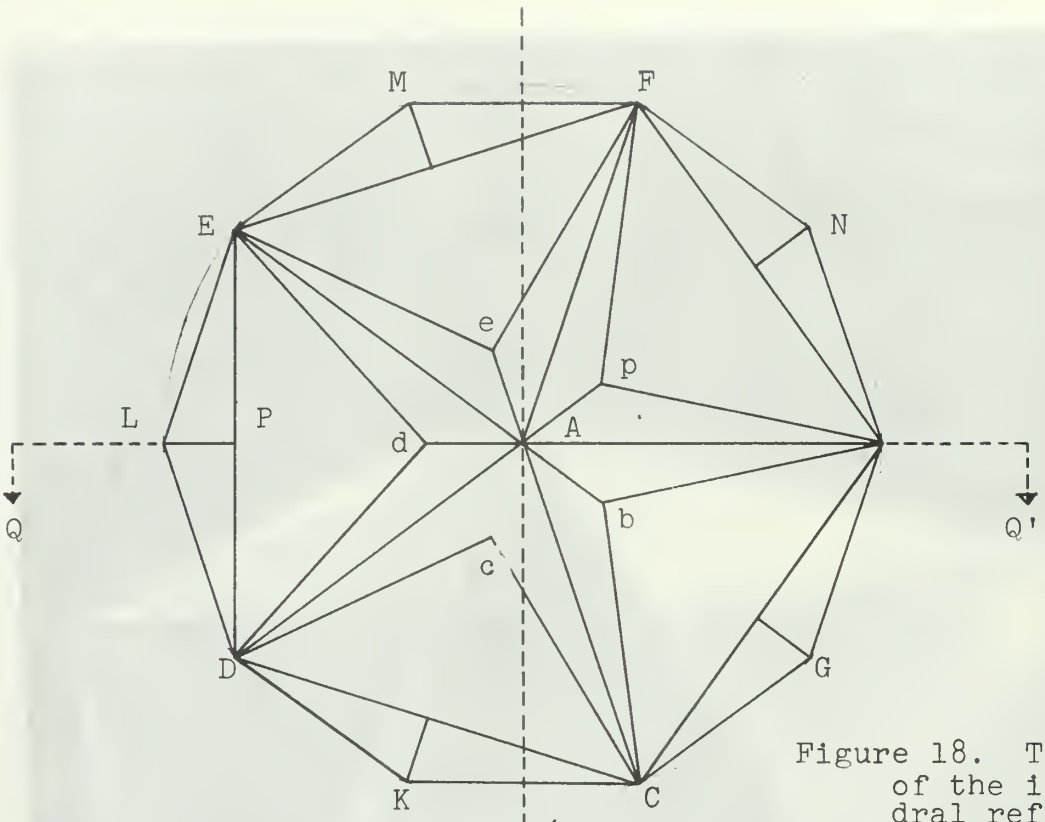

Figure 18. Top view of the icosahedral reflector

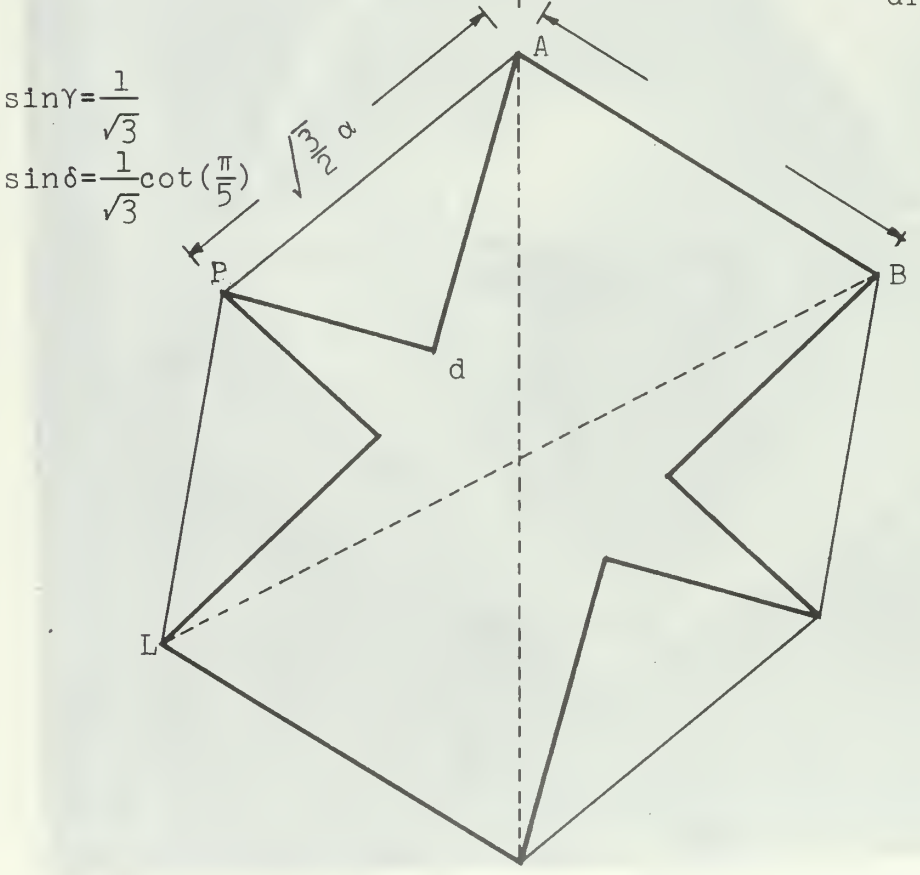

Figure 19. Cross section of the icosahedral reflector on a plane of symmetry

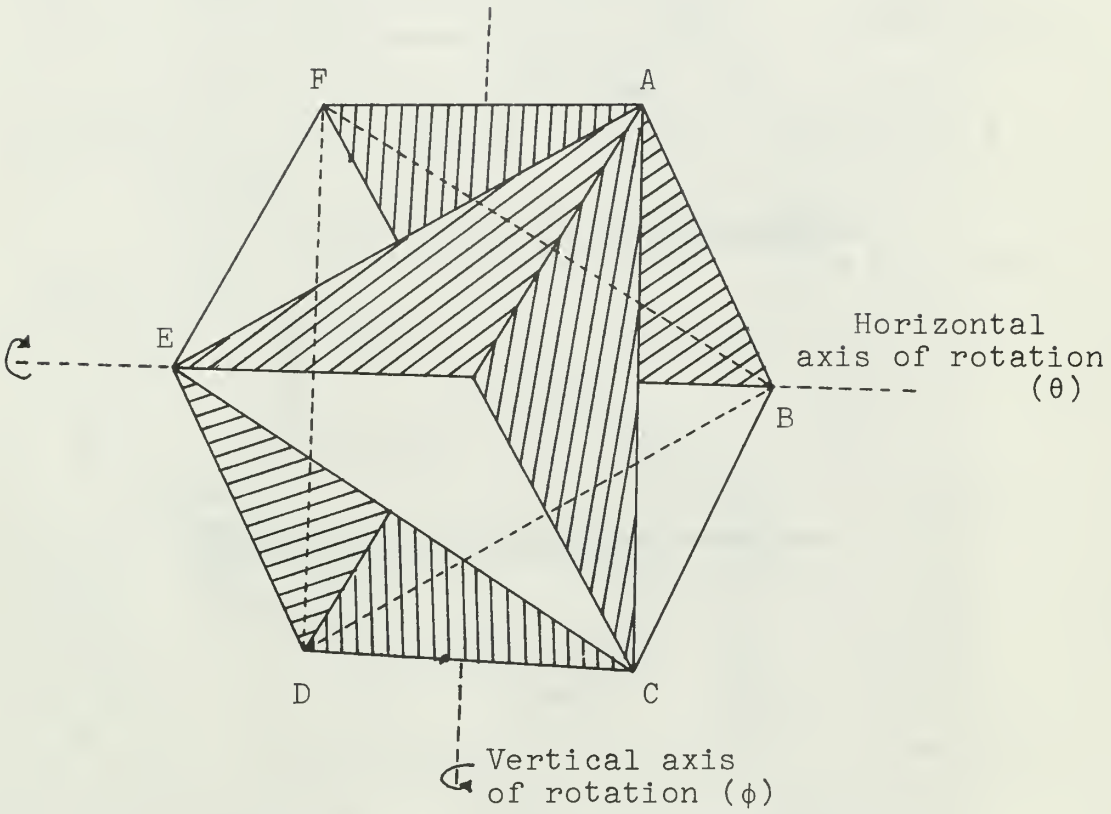

Figure 20. Cluster of eight corner reflection

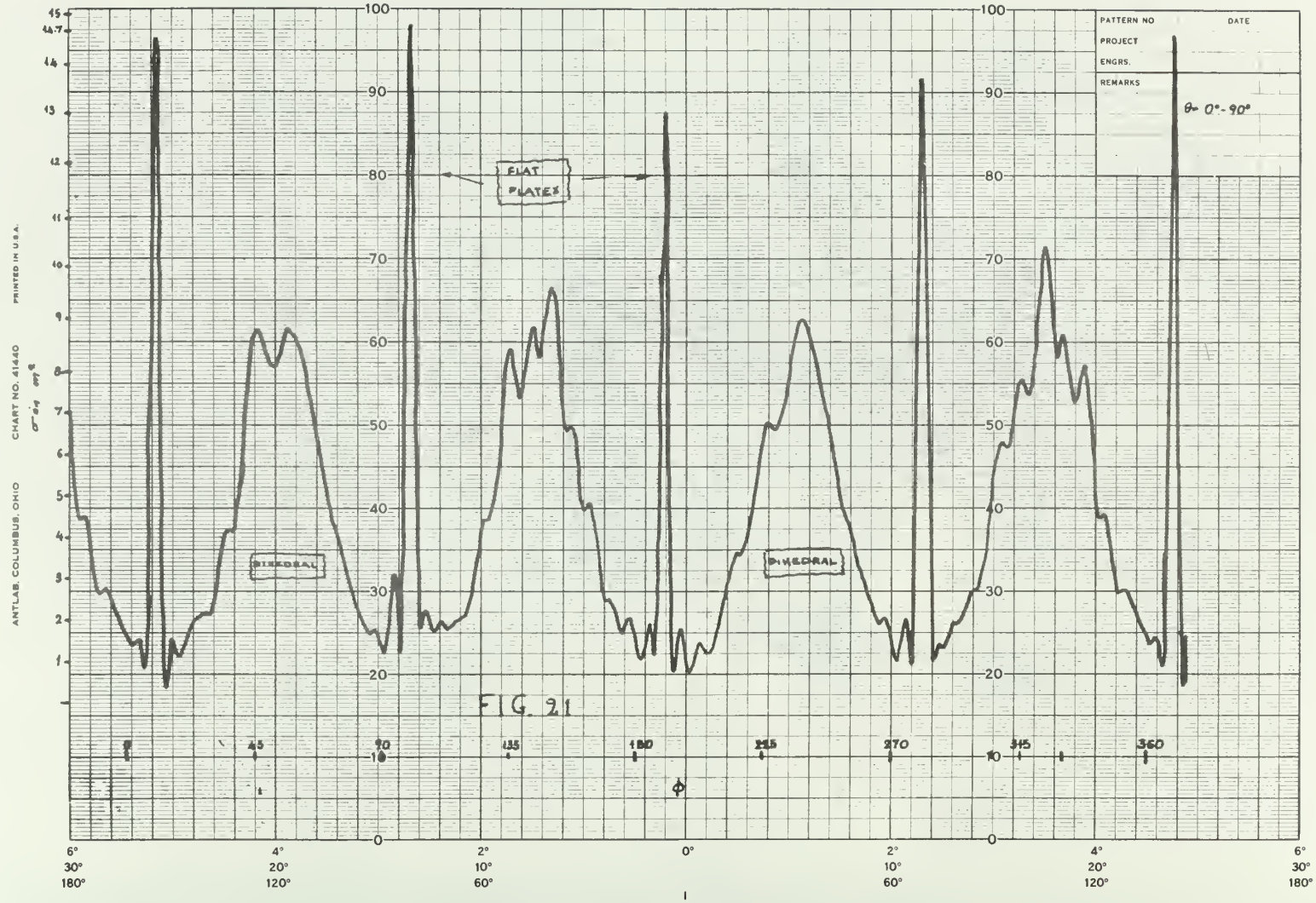
PATTERN NO
DATE
PROJECT
ENGRS.
REMARKS
θ = 0°-90°
FLAT PLATES
DIHEDRAL
DIHEDRAL
ANTLAB, COLUMBUS, OHIO
CHART NO. 41440
PRINTED IN U.S.A.
100
90
80
70
60
50
40
30
20
10
0
45
90
135
180
225
270
315
360
φ
6°
30°
180°
4°
20°
120°
2°
10°
60°
0°
2°
10°
60°
4°
20°
120°
6°
30°
180°

FIG. 21

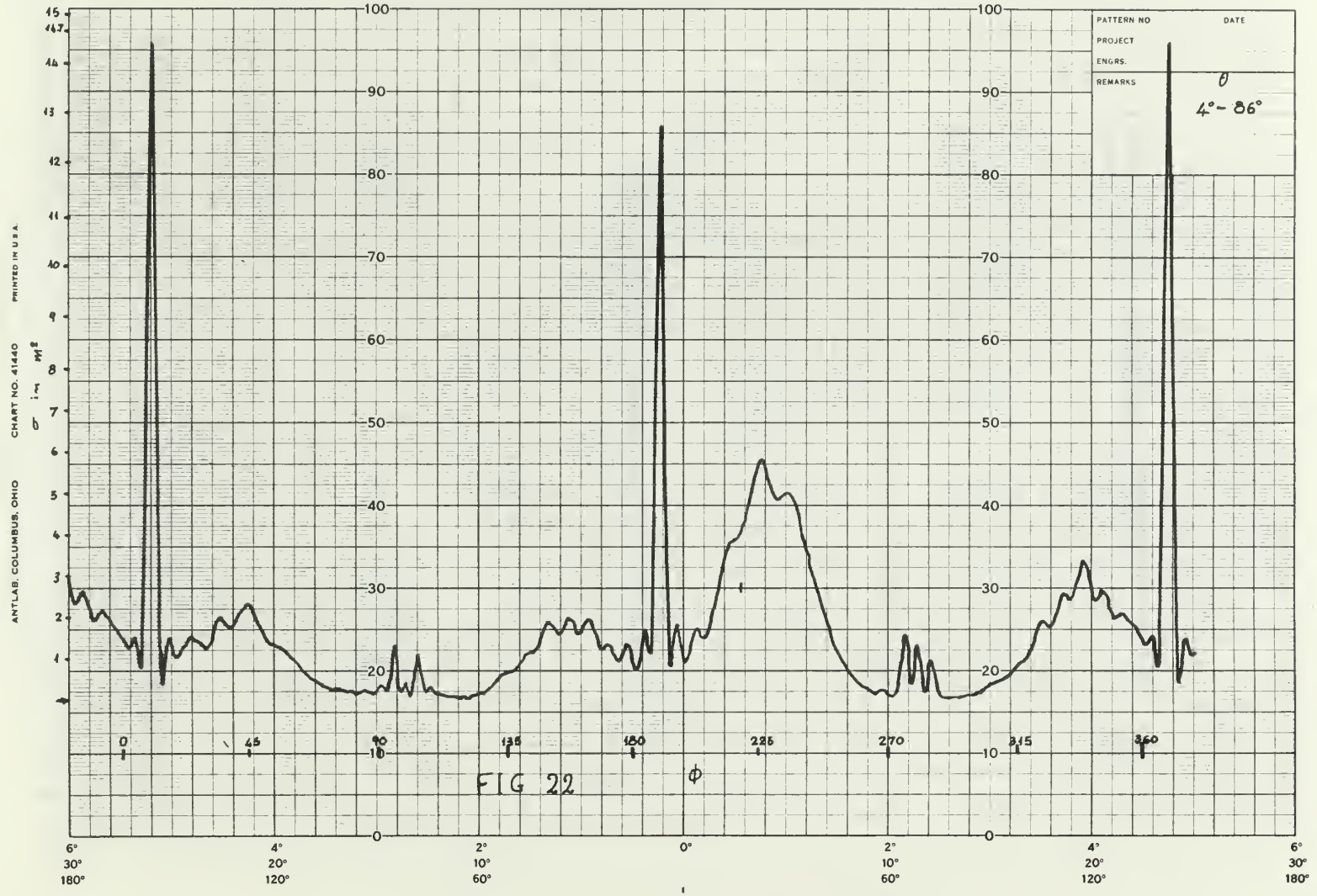
PATTERN NO
DATE
PROJECT
ENGRS.
REMARKS
θ
4°- 86°
ANT LAB, COLUMBUS, OHIO
CHART NO. 41440
PRINTED IN U.S.A.
σ in M²
φ
0
45
90
135
180
225
270
315
360
100
90
80
70
60
50
40
30
20
10
0
6°
30°
180°
4°
20°
120°
2°
10°
60°
0°

FIG 22

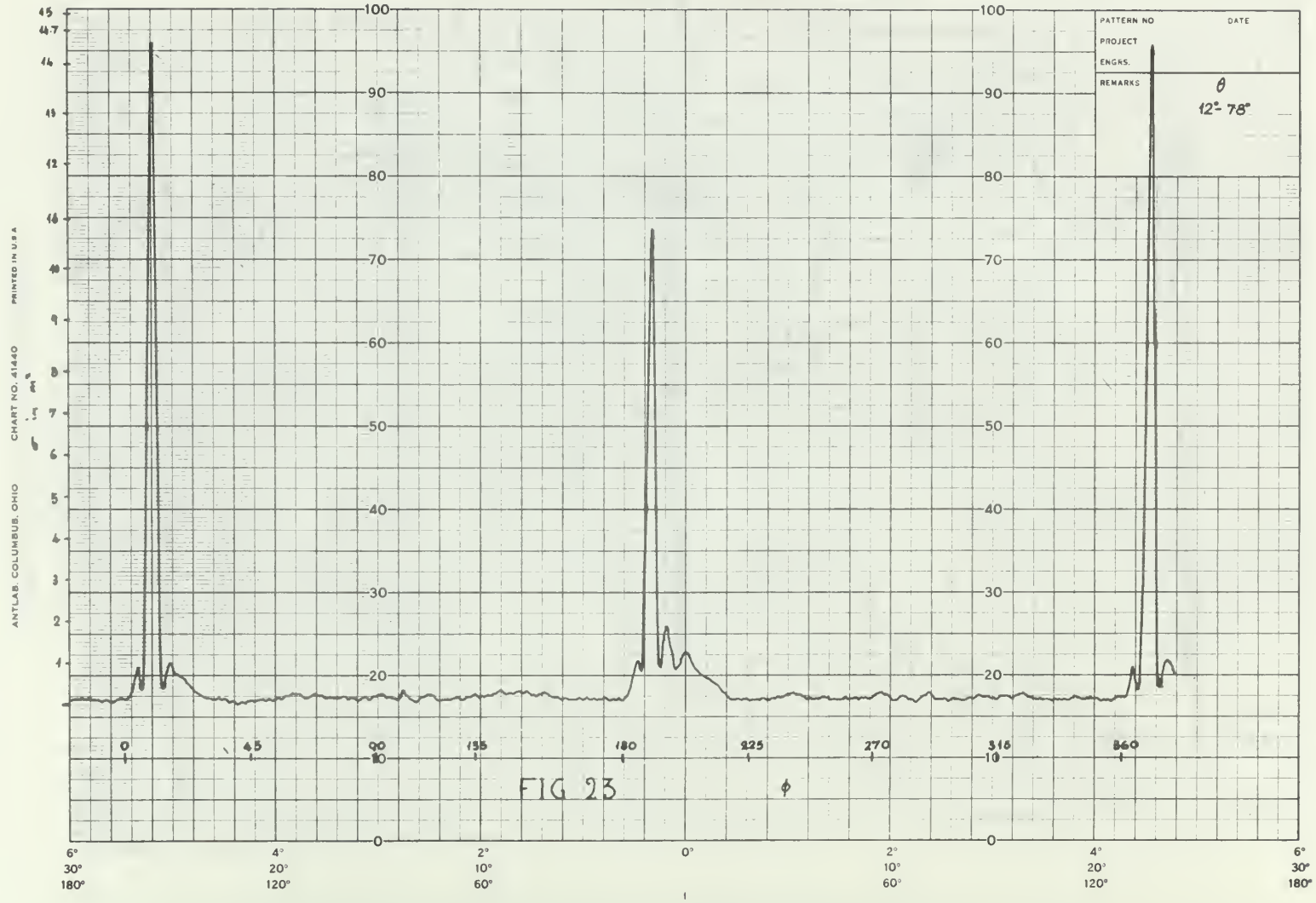
PATTERN NO
DATE
PROJECT
ENGRS.
REMARKS
θ
12°-78°
ANTLAB. COLUMBUS, OHIO
CHART NO. 41440
PRINTED IN U.S.A.
100
90
80
70
60
50
40
30
20
10
0
0
45
90
135
180
225
270
315
360
6°
30°
180°
4°
20°
120°
2°
10°
60°
0°
2°
10°
60°
4°
20°
120°
6°
30°
180°
φ

FIG 23

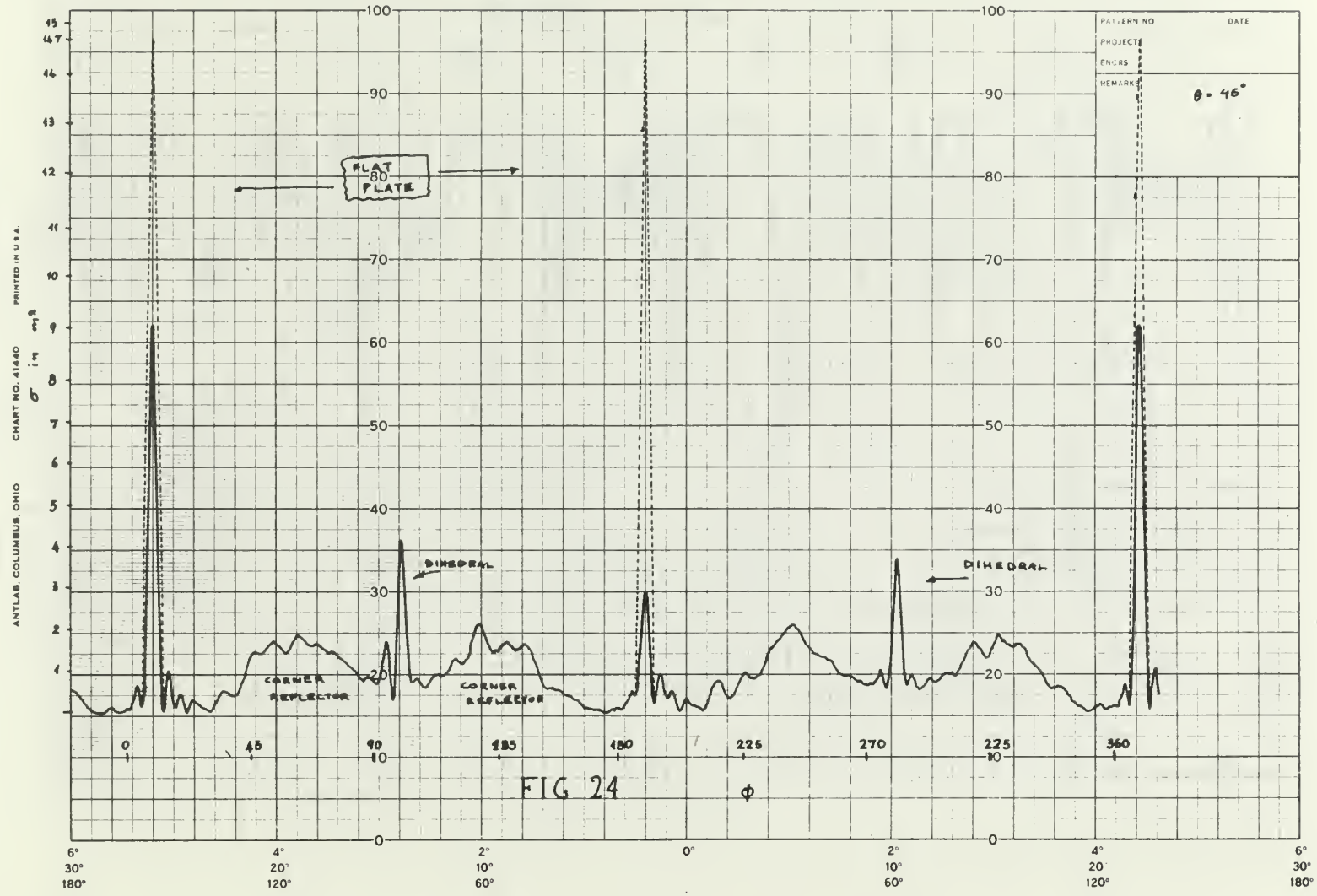
PATTERN NO
DATE
PROJECT
ENGRS
REMARKS
θ = 46°
FLAT PLATE
DIHEDRAL
DIHEDRAL
CORNER REFLECTOR
CORNER REFLECTOR
σ in m²
ANTLAB, COLUMBUS, OHIO
CHART NO. 41440
PRINTED IN U.S.A.
0
45
90
135
180
225
270
225
360
φ
100
90
80
70
60
50
40
30
20
10
0
6°
30°
180°
4°
20°
120°
2°
10°
60°
0°
2°
10°
60°
4°
20°
120°
6°
30°
180°

FIG 24

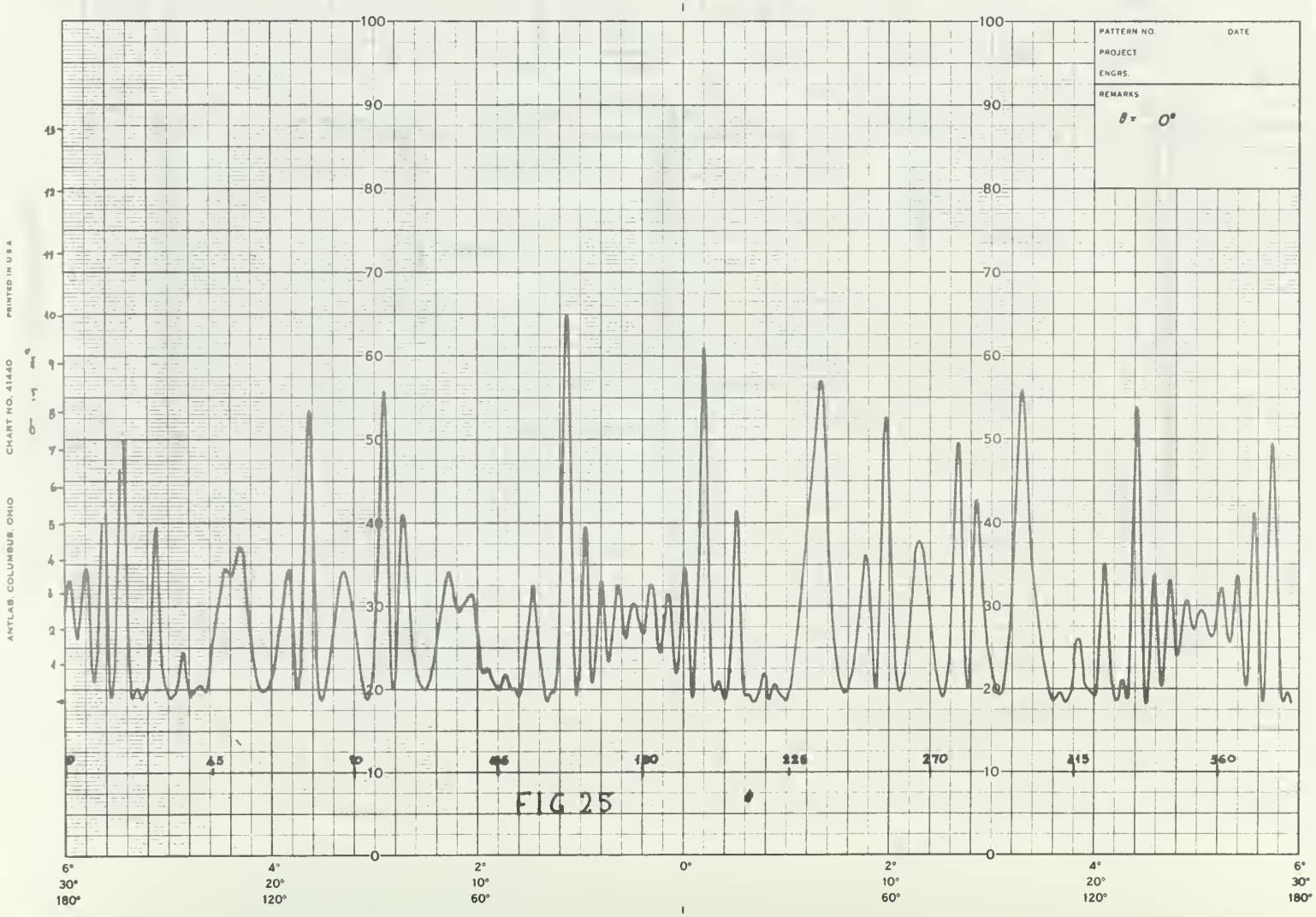
PATTERN NO.
DATE
PROJECT
ENGRS.
REMARKS
θ = 0°
ANTLAB, COLUMBUS, OHIO
CHART NO. 41440
PRINTED IN U.S.A.
100
90
80
70
60
50
40
30
20
10
0
45
90
135
180
225
270
315
360
6°
30°
180°
4°
20°
120°
2°
10°
60°
0°
2°
10°
60°
4°
20°
120°
6°
30°
180°

FIG 25

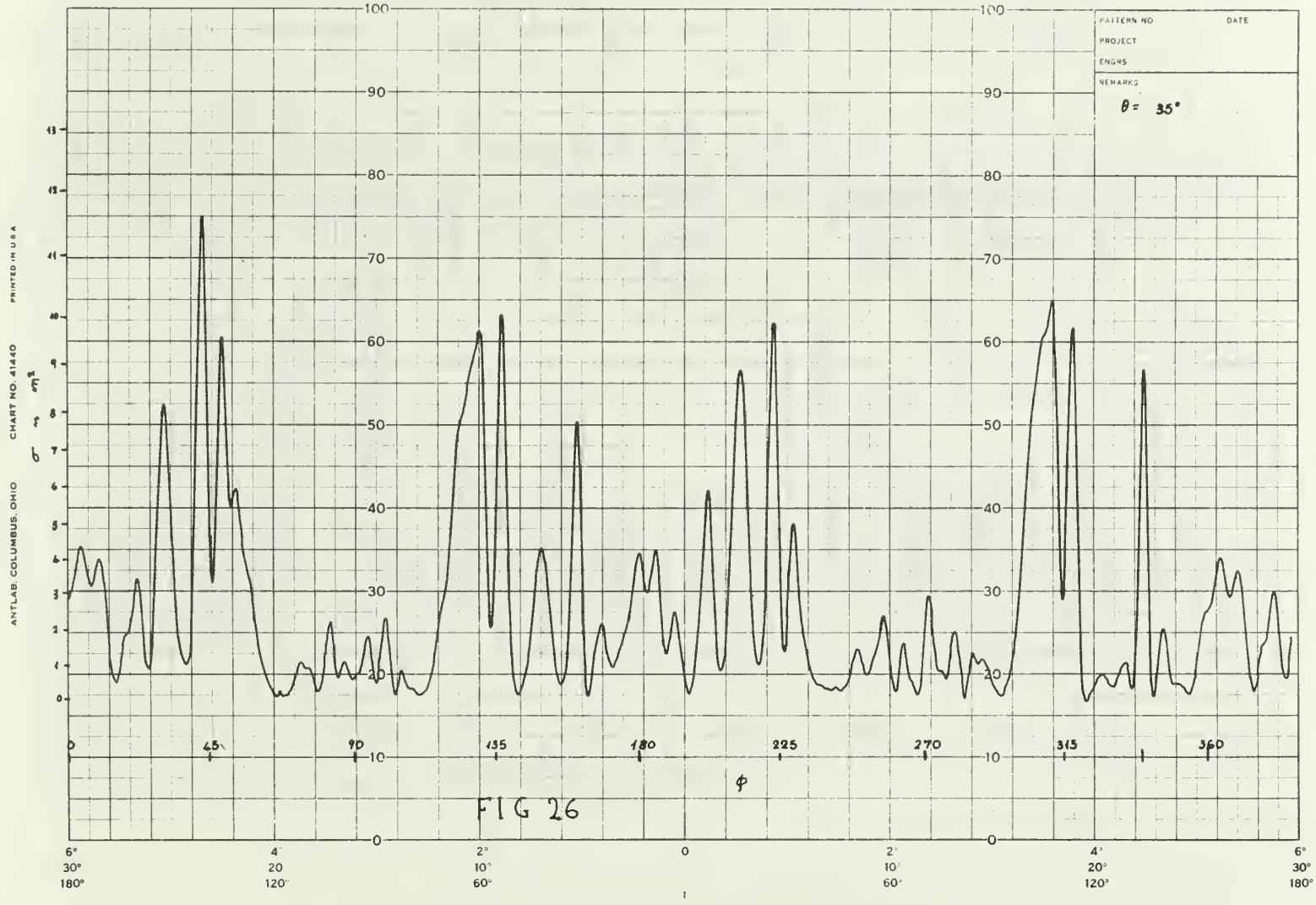
PATTERN NO
DATE
PROJECT
ENGRS
REMARKS
θ = 35°
ANTLAB, COLUMBUS, OHIO
CHART NO. 41440
PRINTED IN U.S.A.
σ in m²
100
90
80
70
60
50
40
30
20
10
0
0
45
90
135
180
225
270
315
360
φ
6°
30°
180°
4°
20
120°
2°
10°
60°
0
2°
10°
60°
4°
20°
120°
6°
30°
180°

FIG 26

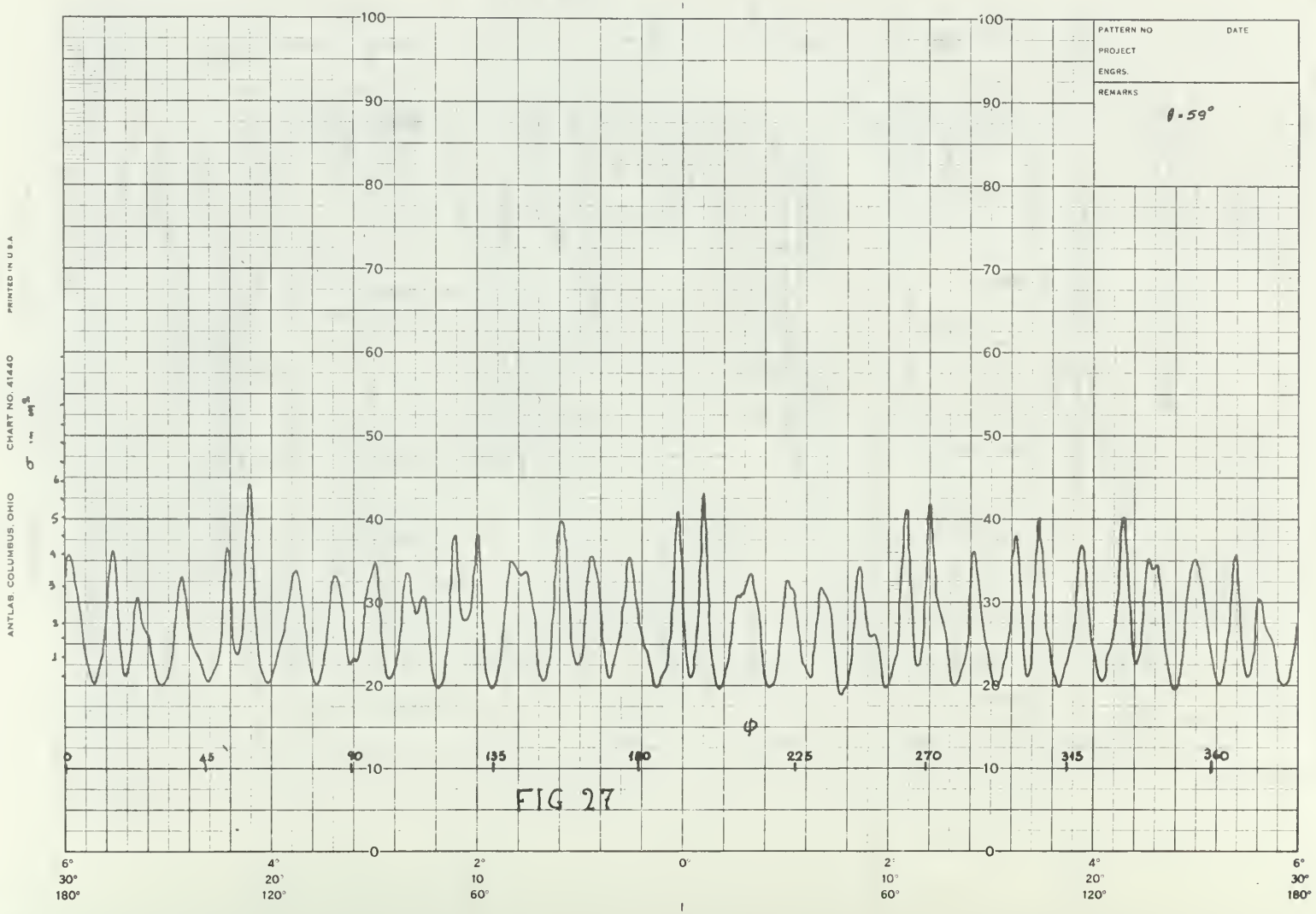
PATTERN NO
DATE
PROJECT
ENGRS.
REMARKS
θ = 59°
ANTLAB, COLUMBUS, OHIO
CHART NO. 41440
PRINTED IN U.S.A.
φ
0
45
90
135
180
225
270
315
360
100
90
80
70
60
50
40
30
20
10
0
6°
30°
180°
4°
20°
120°
2°
10
60°
0°
2°
10°
60°
4°
20°
120°
6°
30°
180°

FIG 27

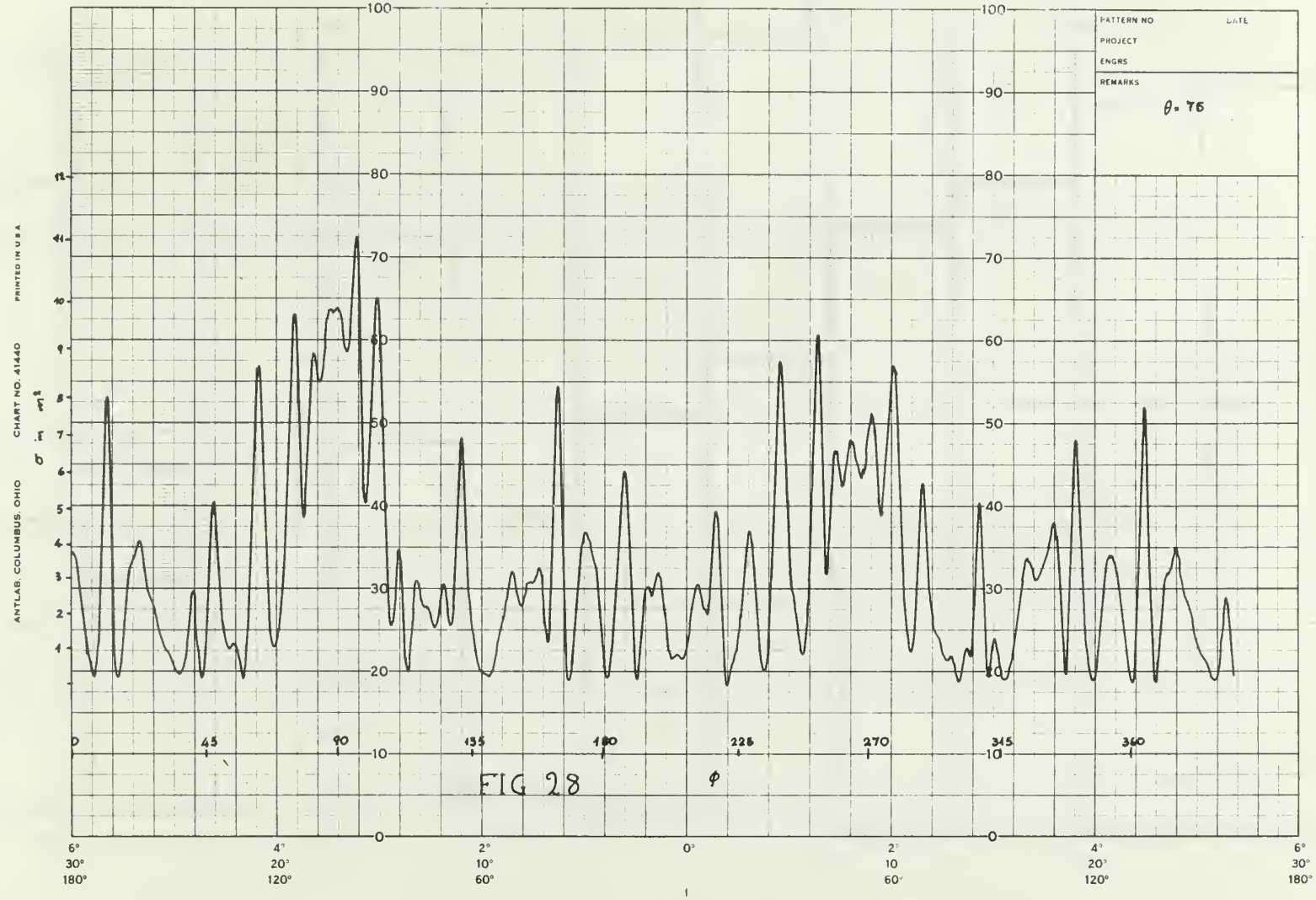
PATTERN NO
DATE
PROJECT
ENGRS
REMARKS
θ = 76
ANTLAB, COLUMBUS, OHIO
CHART NO. 41440
PRINTED IN U.S.A.
σ in m²
100
90
80
70
60
50
40
30
20
10
0
0
45
90
135
180
225
270
315
360
φ
6°
30°
180°
4°
20°
120°
2°
10°
60°
0°
2°
10
60
4°
20°
120°
6°
30°
180°

FIG 28

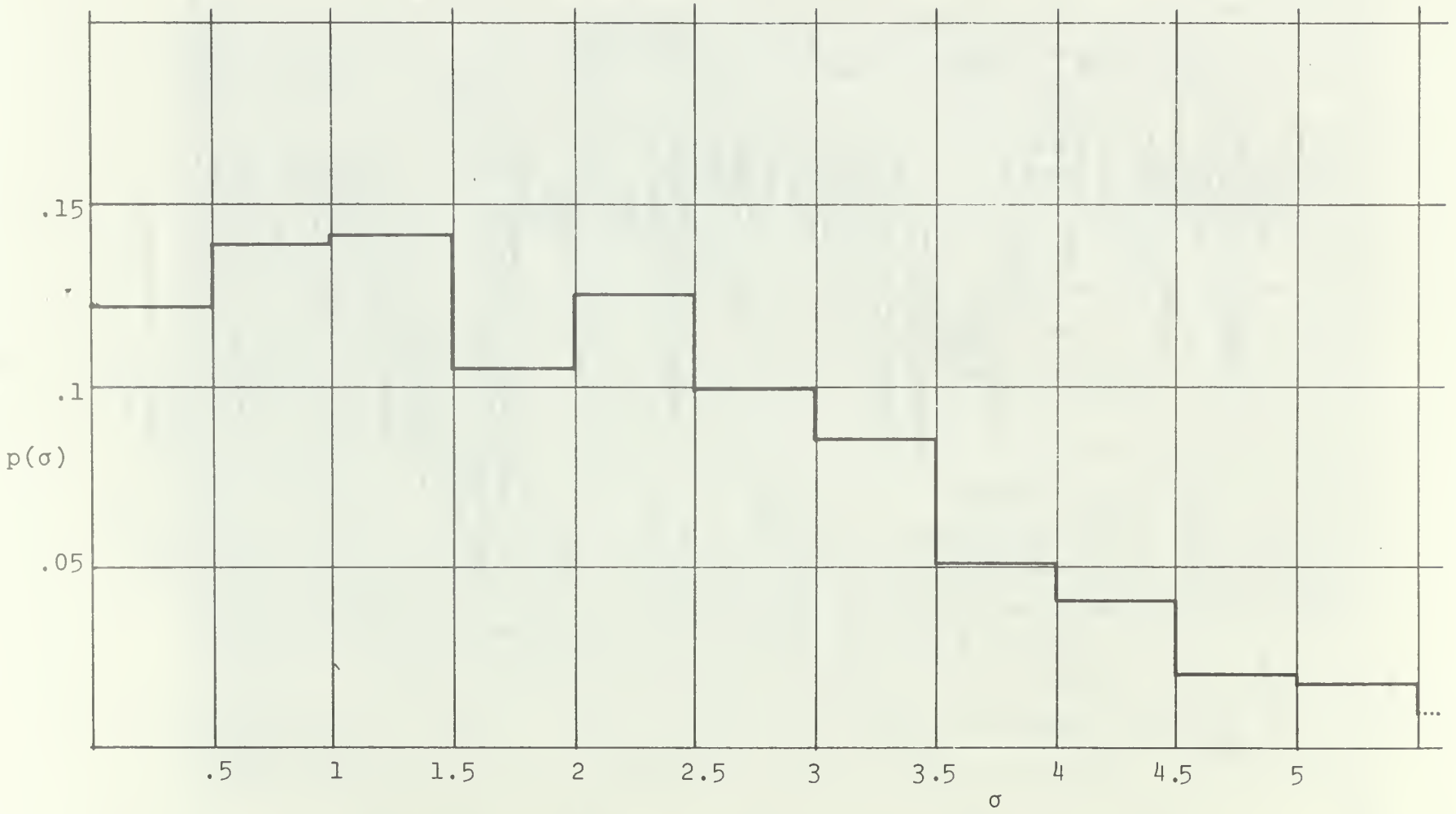

Figure 29. Probability density function of the icosahedral reflector

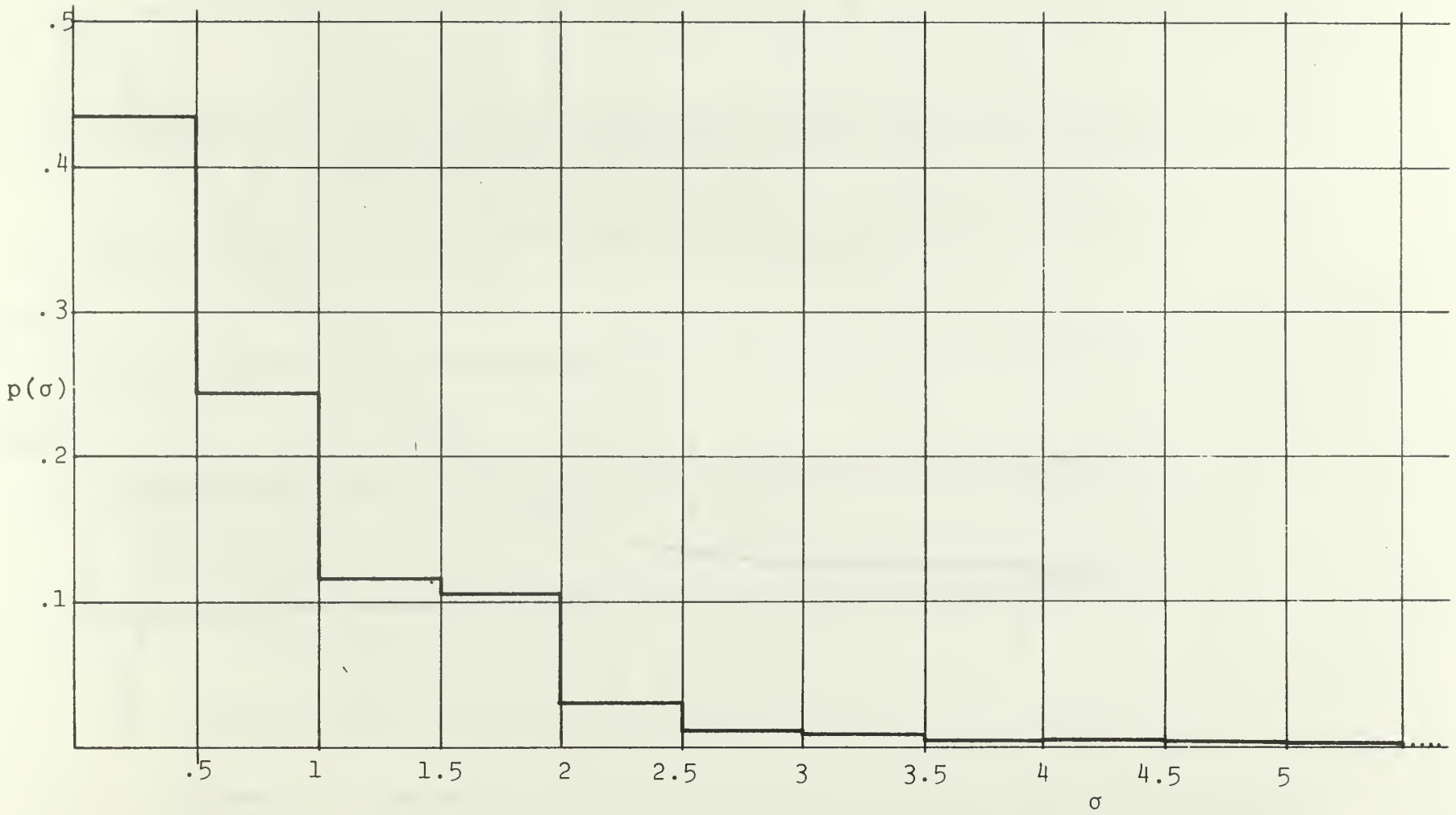

Figure 30. Probability density function of the "standard" reflector

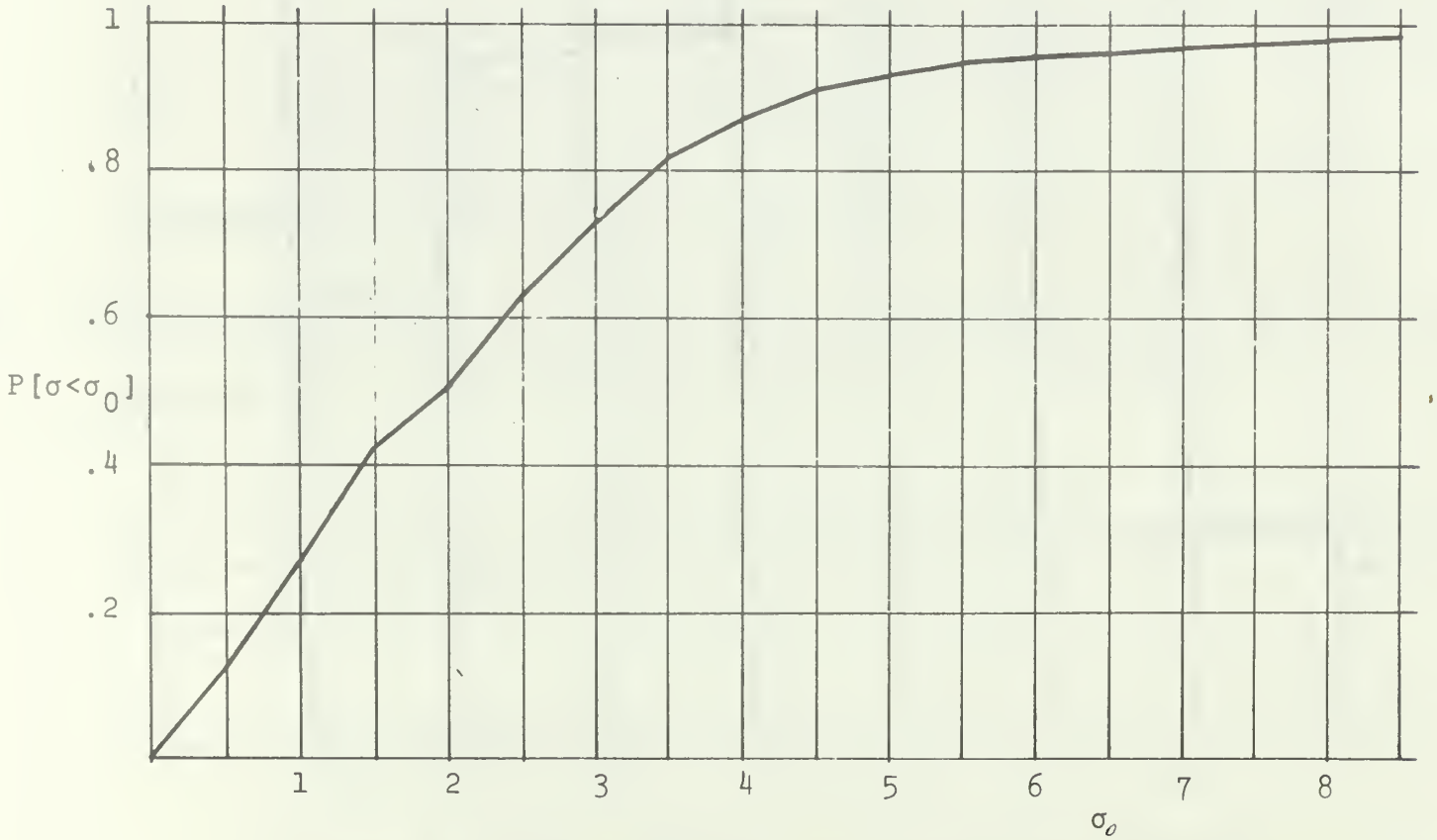

Figure 31. Cumulative distribution function of the icosahedral reflector

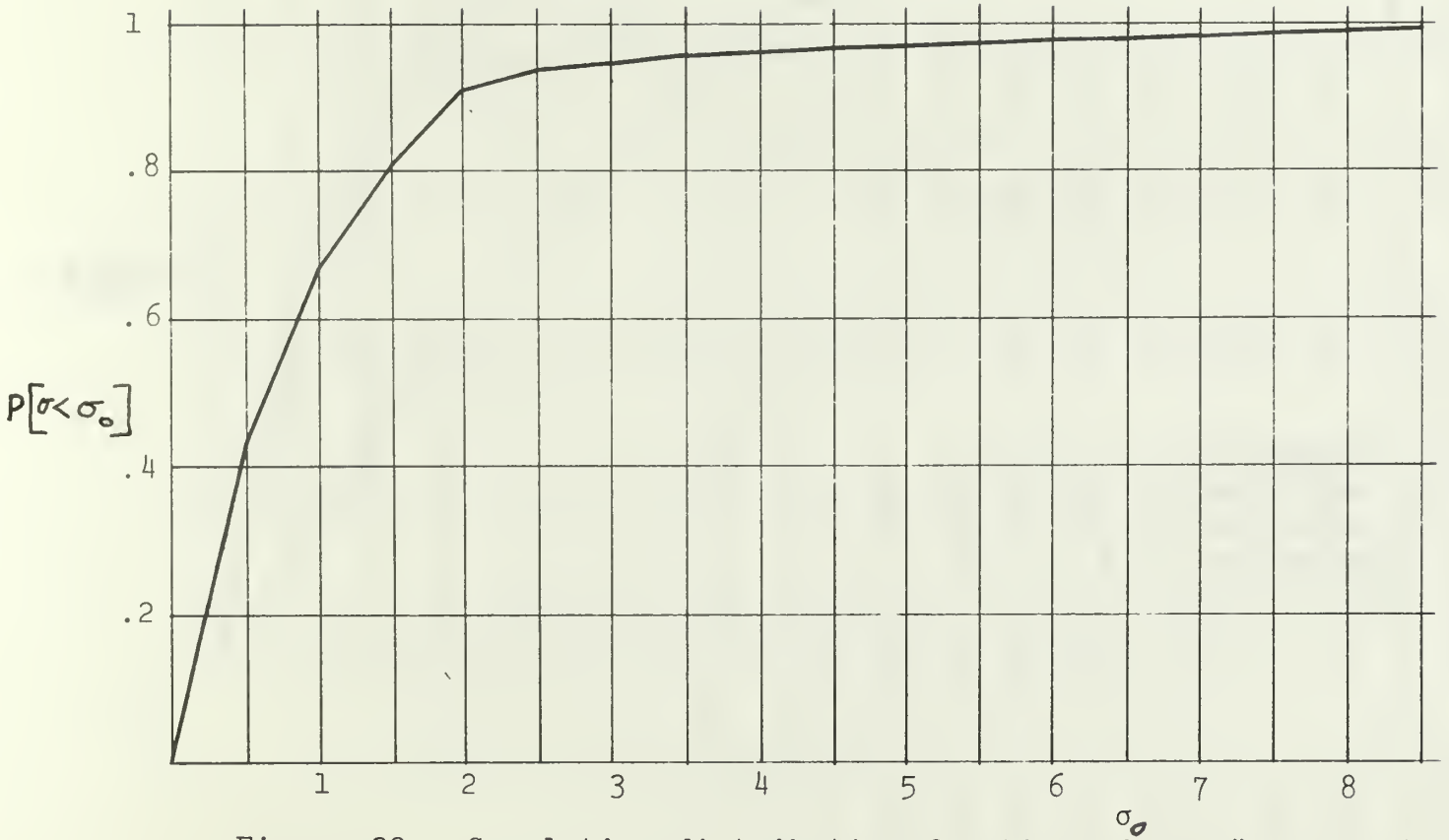

Figure 32. Cumulative distribution function of the "standard" reflector

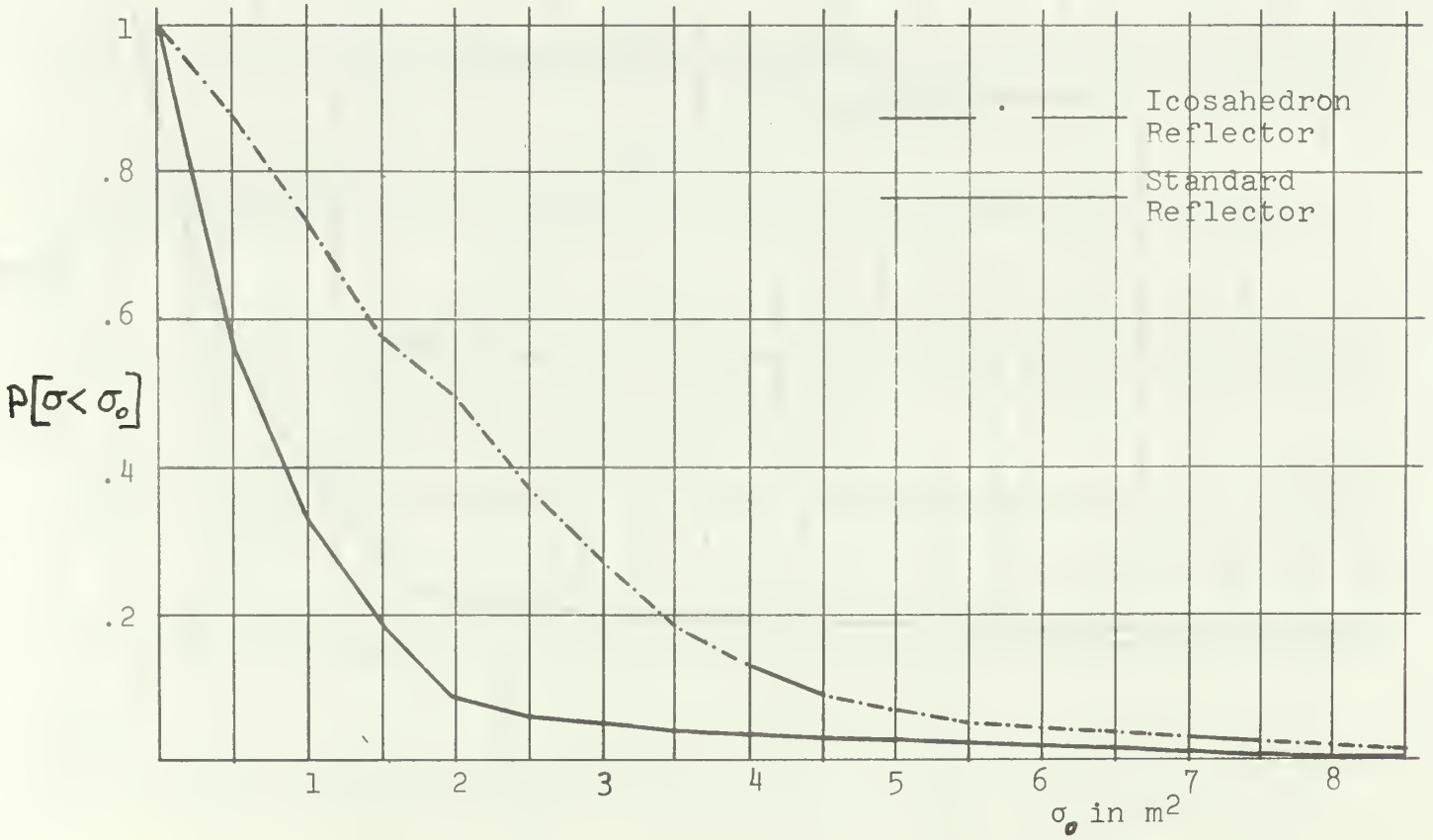

Figure 33. Curves for Comparison of the Reflectors

TABLE I

CALCULATED VALUES OF A AND σ
FOR DIFFERENT ASPECT ANGLES ϕ

ϕ	A'_y/α	B'_y/α	C'_y/α	A'_z/α	$B'_z/\alpha=C'_z/\alpha$	A/α^2	σ^*(in m^2)
0°	0	-.707	.707	.816	-.408	.577	2.58
5°	-.0502	-.755	.655	.816	-.408	.571	2.524
10°	-.1	-.797	.597	.816	-.408	.534	2.215
15°	-.149	-.832	.534	.816	-.408	.473	1.735
20°	-.197	-.862	.468	.816	-.408	.394	1.205
25°	-.244	-.884	.390	.816	-.408	.297	.685
30°	-.289	-.901	.325	.816	-.408	.196	.298
35°	-.331	-.911	.249	.816	-.408	.0895	.0621
39.23°	-.336	-.914	.183	.816	-.408	.448	1.03

*The RCS, σ, was calculated according to the equation

$$\sigma = \frac{4\pi A^2}{\lambda^2}$$

for: $\lambda = 3.33$ cm

$\alpha = 6.364"$

($\alpha = 6.364"$ corresponds to AB = 9")

TABLE II

Interval boundaries σ in m^2	Probability density $p(\sigma)$	Probability distribution $P[\sigma<\sigma_o]$
0 - 0.5	0.1218	0.1218
0.5 - 1.0	0.1388	0.2606
1.0 - 1.5	0.1419	0.4025
1.5 - 2.0	0.1049	0.5074
2.0 - 2.5	0.1253	0.6327
2.5 - 3.0	0.0994	0.7321
3.0 - 3.5	0.0853	0.8174
3.5 - 4.0	0.0512	0.8686
4.0 - 4.5	0.0407	0.9093
4.5 - 5.0	0.0208	0.9301
5.0 - 5.5	0.0176	0.9477
5.5 - 6.0	0.0100	0.9577
6.0 - 6.5	0.0072	0.9649
6.5 - 7.0	0.0064	0.9713
7.0 - 7.5	0.0044	0.9757
7.5 - 8.0	0.0058	0.9815
8.0 - 8.5	0.0036	0.9851
8.5 - 9.0	0.00347	0.9886
9.0 - 9.5	0.00129	0.9917
9.5 - 10.0	0.0017	0.9930
10.0 - 10.5	0.00136	0.9947
10.5 - 11.0	0.0008	0.9967
11.0 - 11.5	0.000287	

TABLE III

Interval boundaries σ in m^2	Probability density $p(\sigma)$	Probability distribution $P[\sigma<\sigma_o]$
0 - 0.5	0.4349	0.4349
0.5 - 1.0	0.2431	0.6780
1.0 - 1.5	0.1261	0.8041
1.5 - 2.0	0.1059	0.9100
2.0 - 2.5	0.0301	0.9401
2.5 - 3.0	0.011	0.9511
3.0 - 3.5	0.0082	0.9593
3.5 - 4.0	0.0045	0.9638
4.0 - 4.5	0.0046	0.9684
4.5 - 5.0	0.0045	0.9729
5.0 - 5.5	0.0036	0.9765
5.5 - 6.0	0.0035	0.9800
6.0 - 6.5	0.00317	0.9832
6.5 - 7.0	0.00167	0.9856
7.0 - 7.5	0.00224	0.9883
7.5 - 8.0	0.00265	0.9917
8.0 - 8.5	0.00244	0.9943
8.5 - 9.0	0.00258	0.9962
9.0 - 9.5	0.00195	0.9979
9.5 - 10.0	0.0017	
10.0 - 10.5	0.000195	
10.5 - 11.0	0.00006	
11.0 - 11.5	0.000093	
11.5 - 12.0	0.000226	
12.0 - 12.5	0.000016	
13.5 - 14.0	0.0002	

III. CONCLUSIONS

Theoretical calculations and experimental measurements have been reported for a single corner reflector. The purpose of this was familiarization with the element used as the basis for the construction of the icosahedral reflector and "standard" octahedral corner reflector, and also for the purpose of checking the performance and accuracy of the experimental setup used.

Having determined the setup's performance to be satisfactory, experimental patterns were taken representing the variation of the radar cross section, σ, with varying aspect for both reflectors, the icosahedron and the "standard" one.

Figure 33 shows at a glance the superiority of the icosahedron. It can be seen that not only is the average RCS of the designed reflector larger, but the probability that σ will be less than one square meter is much less. This later factor is very important, for when the reflector is illuminated by a radar for a brief time, the probability of detection is greatly enhanced if there is high probability that σ is large.

The average cross section of the icosahedron was determined from Figure 29 to be 2.17 m^2, while that of the octahedral reflector is 1.06 m^2. This is a ratio of 2.11, while the cross-sectional areas are in the ratio of 1.81. An even more favorable comparison is obtained from

the ratio of the probability that $\sigma > 1m^2$ in each case, 0.74 vs 0.34, or a ratio of 2.18.

The only case where the icosahedron is at a disadvantage is in a situation where weight is of primary importance. For equal thickness of material, the icosahedron weighs five times as much. In practice, because of the inherent rigidity of this structure it could be made of somewhat lighter material, reducing this disadvantage.

Thus it can be seen that in almost every application where a reflector is desired that will give high reflectivity in all directions, the icosahedral reflector is superior to the conventional octahedral reflector.

APPENDIX

CHARACTERISTICS OF SIMPLY SHAPED RADAR TARGETS

1. SPHERE

Max. effective area: $A_m = a\lambda/2$

Radar cross section: $\sigma = \pi a^2$

Angular response: $\phi = 360$

$\theta = 360$

a = radius

2. CYLINDER

Max. effective area: $A_m = b\sqrt{a\lambda}/2$

Radar cross section: $\sigma = 2\pi ab^2/\lambda$

Angular response: ϕ = 360

θ = sharp

a = radius

b = length

3. FLAT PLATE

Max. effective area: $A_m = a\ b$

Radar cross section: $\sigma = 4\pi a^2 b^2/\lambda^2$

Angular response: ϕ = sharp

θ = sharp

a = width

b = length

LIST OF REFERENCES

1. Crispin, J. W. and Siegel, K. M., Methods of Radar Cross-Section Analysis, p. 71, Academic Press, 1968.

2. Levine, D., Radargrammetry, p. 211-213, McGraw Hill, 1960.

3. Mensa, D., "Elementary Radar Cross Section Properties of Simple Shapes," Naval Missile Center, Point Mugu, California.

4. Jasik, H., Antenna Engineering Handbook, p. 13-8 to 13-10, McGraw Hill, 1961.

5. Brown, S. K., "Effective Area of a Circular Radar Corner Reflector," Office of Naval Research, Naval Research Lab, Washington, D.C.

INITIAL DISTRIBUTION LIST

		No. Copies
1.	Defense Documentation Center Cameron Station Alexandria, Virginia 22314	20
2.	Library, Code 0212 Naval Postgraduate School Monterey, California 93940	2
3.	Professor D. B. Hoisington, Code 52Hs Naval Postgraduate School Monterey, California 93940	1
4.	Lt. Prokopios Katris Chiou 18, Athens 454, Greece	3

DOCUMENT CONTROL DATA - R & D

(Security classification of title, body of abstract and indexing annotation must be entered when the overall report is classified)

1. ORIGINATING ACTIVITY *(Corporate author)*
Naval Postgraduate School
Monterey, California

2a. REPORT SECURITY CLASSIFICATION
Unclassified

2b. GROUP

3. REPORT TITLE
DESIGN AND PERFORMANCE OF A TWENTY-CORNER-CLUSTER REFLECTOR

4. DESCRIPTIVE NOTES *(Type of report and inclusive dates)*
Master's Thesis; December 1969

5. AUTHOR(S) *(First name, middle initial, last name)*
Prokopios Katris, Lieutenant, Royal Greek Navy

6. REPORT DATE
December 1969

7a. TOTAL NO. OF PAGES
70

7b. NO. OF REFS
5

8a. CONTRACT OR GRANT NO.

b. PROJECT NO.

c.

d.

9a. ORIGINATOR'S REPORT NUMBER(S)

9b. OTHER REPORT NO(S) *(Any other numbers that may be assigned this report)*

10. DISTRIBUTION STATEMENT
This document has been approved for public release and sale; its distribution is unlimited.

11. SUPPLEMENTARY NOTES

12. SPONSORING MILITARY ACTIVITY
Naval Postgraduate School
Monterey, California 93940

13. ABSTRACT

This paper is a report on the design and performance of a twenty-corner-cluster (icosahedron) reflector.

Comparison of the measured cross sections of the icosahedron reflector with those of a cluster of eight corner reflectors used as a "standard" reflector shows the former being superior in performance over the latter in that it gives nearly omnidirectional response.

DD FORM 1 NOV 65 1473 (PAGE 1)
S/N 0101-807-6811

A-31408

14. KEY WORDS	LINK A		LINK B		LINK C	
	ROLE	WT	ROLE	WT	ROLE	WT
TWENTY-CORNER-CLUSTER REFLECTOR (ICOSAHEDRAL REFLECTOR)						
CORNER REFLECTOR						
DIHEDRAL REFLECTOR						
RADAR CROSS SECTIONS						
EFFECTIVE AREA OF TARGETS						

thesK1453
Design and performance of a twenty-corne
3 2768 001 02855 8
DUDLEY KNOX LIBRARY